

# UC Berkeley

## UC Berkeley Electronic Theses and Dissertations

### Title

Allosteric Substrate Switching in Novel Voltage Sensing Lipid Phosphatase

### Permalink

<https://escholarship.org/uc/item/41v8884p>

### Author

Grimm, Sasha Shekhar

### Publication Date

2015

Peer reviewed|Thesis/dissertation

Allosteric Substrate Switching in Novel Voltage Sensing Lipid Phosphatase

by

Sasha Shekhar Grimm

A dissertation submitted in partial satisfaction of the

requirements for the degree of

Doctor of Philosophy

in

Biophysics

in the

Graduate Division

of the

University of California, Berkeley

Committee in charge:

Professor Ehud Y. Isacoff

Professor Terry E. Mackin

Professor Polina Lishko

Professor John E. Deuber

Spring 2015



Abstract

## Allosteric Substrate Switching in Novel Voltage Sensing Lipid Phosphatase

by

Sasha Shekhar Grimm

Doctorate of Philosophy in Biophysics

University of California, Berkeley

Professor Ehud Y. Isacoff, Chair

The explosion of protein diversity through domain rearrangements and inter-domain coupling supported the evolution of multicellular organisms. To perform the advanced signaling necessary for multi-cellularity, sometimes-unrelated protein domains combined to form novel domain architectures that over time evolved tight mechanisms of allosteric coupling. One such protein, the voltage sensing phosphatase (VSP), developed a sophisticated mechanism of inter-domain coupling, which enabled cells to integrate changes in membrane potential into chemical changes in a class of secondary signaling lipids called phosphatidylinositol-phosphates (PIPs).

Phosphoinositol phosphate signaling lipids (PIPs) are important second messengers that regulate ion channels, transporters, cell motility and endo/exocytosis. PIP concentrations are controlled by enzymes, including VSP, which has broad specificity for a diverse class of PIPs. VSP is a novel lipid phosphatase, which contains a voltage sensing domain (VSD) homologous to voltage-gated ion channels, and a lipid phosphatase domain (PD). Until now it was not known what properties of the cytosolic PD were allosterically regulated by the membrane-associated VSD. Using fast PIP sensors to monitor enzyme activity and voltage clamp fluorometry to monitor conformational changes in the VSD, it becomes clear that the *Ciona intestinalis* VSP (Ci-VSP) has two distinct voltage regulated enzyme active states: a faster low-voltage state with substrate preference for PIP<sub>3</sub> and a slower high-voltage state with preference for PIP<sub>2</sub>. This novel 2-step allosteric switch for enzyme specificity enables membrane potential to function as an allosteric effector that dynamically regulates PIP concentration.

In this work, it is shown that two unrelated domains, a VSD from voltage dependent ion channels and a lipid PD homologous to protein tyrosine phosphatases evolved a tight mechanism of allosteric regulation that transduces fluctuations in membrane potential into changes in the enzyme selectivity of a novel lipid phosphatase. This regulation of active site specificity in the PD by an allosteric effector domain represents a significant advancement in our understanding of allosteric regulation, which has previously been restricted to control of activity on only one type of substrate.

## Table of Contents

|  |     |
|--|-----|
| Acknowledgements.....  | iii |
| INTRODUCTION .....   | 1   |
| PROTEIN DOMAINS and EVOLUTION .....  | 1   |
| Domain modularity and VSP.....   | 1   |
| VSP and the origins of multi-cellularity.....  | 1   |
| SENSING MEMBRANE POTENTIAL.....  | 3   |
| Introduction to membrane potential .....   | 3   |
| Quantitative look at membrane potential.....   | 3   |
| History of the voltage sensing domain .....  | 5   |
| The voltage sensing domain and VSP .....   | 6   |
| CHEMICAL CHANGES IN THE CELL .....   | 9   |
| PIPs and the potential function of VSPs.....   | 9   |
| Overview of protein tyrosine phosphatases.....   | 9   |
| Phosphatase domain and linker in VSP.....  | 9   |
| FIGURES .....  | 11  |
| Figure1. Protein Domains and Evolution. ....   | 11  |
| Figure2. VSD evolution.....  | 12  |
| Figure3. Sequence alignment of VSD across species.....                                   | 13  |
| Figure4. Domain architecture of VSD-containing proteins.....                             | 14  |
| Figure5. VCF reports changes in the VSD .....  | 15  |
| Figure6. Kinetics of 214* show properties of Hodgkin and Huxley gating particle.....     | 16  |
| ALLOSTERIC SUBSTRATE SWITCHING IN VOLTAGE SENSING PHOSPHATASE.....                       | 17  |
| ABSTRACT:.....   | 17  |
| INTRODUCTION:.....   | 18  |
| RESULTS.....   | 20  |
| New fast PIP <sub>2</sub> reporters.....   | 20  |
| Wildtype Ci-VSP appears to transition sequentially between two distinct enzymatic states | 20  |
| Sequential conformational changes in the VSD and state-stabilizing mutants .....         | 21  |
| VSD mutants favor A1 or A2 state of the PD .....   | 22  |
| VSD conformations in inactive and active states of PD.....                               | 23  |
| DISCUSSION .....   | 24  |
| FIGURES .....  | 25  |

|  |    |
|--|----|
| Figure1. Wildtype Ci-VSP appears to have two active enzymatic states.....                | 25 |
| Figure2. Stabilization of discrete conformations in the gating plug of VSD. ....         | 26 |
| Figure3. VSD mutants stabilize discrete VSD conformations. ....                          | 27 |
| Figure4. VSD mutants stabilize discrete enzyme activity states. ....                     | 28 |
| Figure5. Two-step VSD control over VSP phosphatase with two active states.....           | 29 |
| Supplemental Figure1. Membrane associated FRET reporters faster than cytosolic.....      | 30 |
| Supplemental Figure2. Mean change in FRET. ....  | 31 |
| Supplemental Figure3. Endogenous Activity in Xenopus Oocytes. ....                       | 32 |
| Supplemental Figure4. Single sigmoidal fits for double sigmoid. ....                     | 33 |
| Supplemental Figure5. Stabilization of VSD using interactions below the VSD plug. ....   | 34 |
| Supplemental Figure6. Activity data for Ci-VSP single mutants.....                       | 35 |
| Supplemental Figure7. Ci-VSP has 5-position phosphatase preference at all voltages. .... | 36 |
| Supplemental Figure8. Representative traces resemble average from multiple cells. ....   | 37 |
| METHODS.....   | 38 |
| Molecular Biology.....   | 38 |
| Fluorescence Measurement of Activity.....  | 38 |
| Voltage Clamp Fluorometry.....   | 39 |
| REFERENCES .....   | 40 |

## Acknowledgements

*“Do not be too timid and squeamish about your actions. All life is an experiment. The more experiments you make the better. What if they are a little course, and you may get your coat soiled or torn? What if you do fail, and get fairly rolled in the dirt once or twice? Up, again, you shall nevermore be so afraid of a tumble.”*

– Ralph Waldo Emerson

Accepting failure and mustering the optimism to start again is an inevitable part of experimentation. Building the endurance to pursue a research hypothesis past idealistic aspirations through rotten low hanging fruit and into a verifiable and enduring finding takes persistence, self-mastery and a strong support system. The success of this project was possible because of the guidance and encouragement I received from the friends, family, advisors, and colleagues that helped me up and dusted me off when I got “rolled in the dirt once or twice.”

Good quality research guidance doesn’t need to take a lot of time. Of upmost significance to this project was the support of my advisor. Udi provided me with the independence I needed to establish my confidence as a scientist, while also giving subtle hints and encouragement that prevented me from becoming discouraged. This dissertation is a direct product of the discussions Udi and I had while putting together our manuscript. Working to distill and refine my experiments into this cohesive finding was the highlight of my time in the lab.

Discussion with colleges and the work of our predecessors shape and refine our thinking as scientists. The colleagues I worked with over the five years I spent in the Isacoff lab were key to the progress of this work and my development as a scientist. Research done by Susy and Sarah, my predecessors, laid the groundwork in the lab and the field at large, without their preliminary work this project would not have been plausible. Regular discussions and debates with Andreas and Beth about science as well as non-science related topics were also a formative part of the timely progression of this research; our discussions clarified my thinking and supported my development as a scientist.

We test hypotheses, but the complexity of nature tests persistence and rewards grit. When I was frustrated by months of troubleshooting noise and failed attempts to get an impossible assay to work, or if an important set of experiments went poorly, I always called home. During these difficult times my mom would listen and talk me through my frustration, while my dad offered his support by reminding me how far I’d come and that each setback (or challenge) was not failure but an incremental part of the progress.

A healthy life outside the lab is important to progress in the lab. Late nights and early mornings as well as the frustrations that are an inevitable part of graduate school can take a toll on any relationship. My dear husband faithfully championed my endeavors, he provided emotional support when I needed it but also inspired me to pursue productive ways of managing my stress. Finding a balance between working hard and playing hard made it possible to pursue this project past difficulties, like getting scooped, and into a project of substance and real scientific value.

## INTRODUCTION

The explosion of protein diversity through domain rearrangements and inter-domain coupling supported the evolution of multicellular organisms. To perform the advanced signaling necessary for multi-cellularity, sometimes-unrelated protein domains combined to form novel domain architectures with tight mechanisms of allosteric coupling. One such protein, the voltage sensing phosphatase (VSP), developed a sophisticated mechanism of inter-domain coupling, which enabled cells to integrate changes in membrane potential into chemical changes in a class of secondary signaling lipids called phosphatidylinositol-phosphates (PIPs). In this work, I present evidence that two unrelated domains, a voltage sensing domain (VSD) from voltage dependent ion channels and a lipid phosphatase domain (PD) homologous to protein tyrosine phosphatases (PTPs), evolved a tight mechanism of allosteric regulation that transduces fluctuations in membrane potential into changes in the enzyme selectivity of a novel lipid phosphatase.

## PROTEIN DOMAINS and EVOLUTION

### Domain modularity and VSP

Protein domains are independent functional units that combine to form multi-domain proteins with diverse architecture and functions. These domains can arrange and assemble in novel ways as a result of genetic events like gene duplication, gene fusion and gene fission(1, 2). Under selective pressure, the resulting proteins evolve new or specialized functions, which are selected for and conserved through evolutionary time(3-5). More simply, protein domains function like logic gates in a biological circuit, input domains detect a signal that is then relayed to an output domain that is activated at a distance(3, 6); once activated (or inactivated) the protein produces a cellular response. The modular independent protein domains rearrange into different structural contexts that are rediscovered by evolution.

The concept of domain modularity is best understood in the context of a single protein. One particularly good example of inter-domain coupling exists between two of the domains in the voltage sensing phosphatase (VSP). VSP contains three domains; a transmembrane voltage sensing domain (VSD), a lipid phosphatase domain (PD), and a C2 domain. The VSD is homologous to the voltage sensing domains found in voltage dependent ion channels, and the lipid phosphatase domain is homologous to the protein tyrosine phosphatase superfamily of proteins(7-10). The C2 domain is less relevant to this study, but it may also play a role in enzyme activity(11). In the pages that follow it is shown that two otherwise unrelated domains, the VSD and PD, evolved a very tight mechanism of allosteric coupling.

### VSP and the origins of multi-cellularity

The 37.2 trillion cells(12) of the human body rely on proteins and signaling pathways to integrate signals across cells. One of the most critical is the phosphotyrosine signaling pathway which appeared shortly before the evolution of multi-cellularity ~600 million years ago(13, 14). This pathway is described as having three modular domains; a *writer* (tyrosine-kinase, TyrK), *eraser* (protein tyrosine-phosphatase PTP) and *reader* (Sh2 domain). These three components work together to form an array of complex circuits that control communication between cells and regulate critical cellular processes(15-17).

Proteins containing sophisticated domain architectures with combinations of the *writer/eraser/reader* domains did not exist in simple organisms like yeast and slime mold but are abundant in the genomes of animals (metazoan) and choanoflagellates, a species of unicellular



organisms that assemble into multicellular colonies (**Fig.1**). It is therefore speculated that the evolution of multi-cellularity required an increase in the domain complexity of phosphotyrosine signaling proteins(16). Similarly, the domain architecture of VSP, which consists of an *eraser* domain and a voltage sensing domain from ion channels, is also found only in the metazoan (animals) and choanoflagellate genomes (**Fig. 2**)(7, 14, 18) and may have evolved during the same expansion in domain architecture diversity.

The phosphatase domain of VSP is a member of the PTP/*eraser* component of the phosphotyrosine signaling system but unlike most PTPs which remove phosphates from proteins, VSP functions as a lipid phosphatase and removes phosphates from the head group of phosphatidylinositol signaling lipids (PIPs)(7, 19-22). The regulatory effects induced by binding of PIP head groups to cytosolic and membrane proteins perform functions analogous to the *reader* component of the phosphotyrosine signaling pathway,(16, 23) so it can be further suggested that PIP modulation through VSP may function as a parallel part of the phosphotyrosine signaling pathway – with the writer being the PIP substrate and the eraser being the PTP of VSP; both processes integrate signals at the membrane cytosol and regulating cell interactions in response(24).

Taken together, our observations suggest that VSP evolved during an evolutionary explosion in protein diversity, which exploited domain modularity to form novel domain architectures. Since this occurred around the time organisms evolved sophisticated phosphotyrosine signaling pathways and this protein integrates changes in membrane potential with related chemical signaling process in the cell, it may have been a critical part of the cellular regulation mechanisms essential to multi-cellularity.

## SENSING MEMBRANE POTENTIAL

### Introduction to membrane potential

The voltage sensing phosphatase senses changes in membrane potential and translates these changes into enzyme activity. Detection of membrane potential occurs through the voltage-sensing domain (VSD), a domain that first appeared in single cellular organisms as part of the voltage dependent ion channels. Ion channels, similar to enzymes, catalyze important physiological processes by controlling the movement of ions across the cellular membrane (1, 8, 25). The cell membrane is selectively permeable; it allows some molecules to diffuse passively through but relies on passive and active transport mechanisms to regulate permeability.

Ions are charged and do not readily diffuse across the hydrophobic membrane environment, thus ion conduction must rely on transport through pores. The density of these active and passive transport proteins, their affinity and selectivity for particular ion substrate, as well as their tendency to be active over inactive, collectively dictate the electrochemical properties of the cell membrane (1, 3, 8). At rest, the ions in a living cell are in a dynamic steady state with a relatively stable difference in the bulk concentration of potassium, sodium and chloride ions on inside of the cell versus the outside; ions are still moving in and out of the cell through ion channels and transporters but the number of ions moving in is roughly equal to the number of ions going out. At the membrane interface the separation of charge that exists at steady state creates a local electrical field this is detected by proteins located in or very near the membrane, these proteins undergo structural changes in response to changes in the electric field.

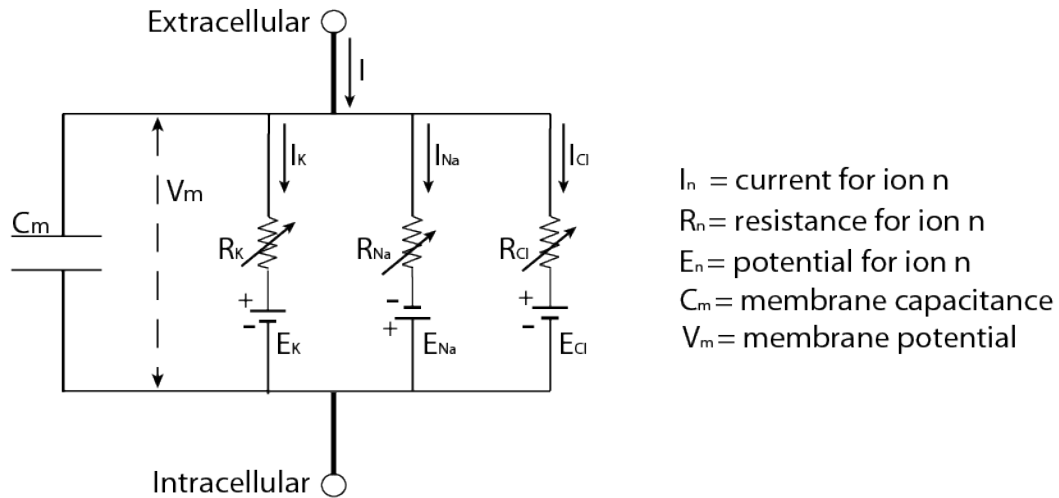
The difference in membrane potential is created by ions in the cell. Potassium ( $K^+$ ) is the most membrane permeable of the three ions, diffusion of potassium ions from the inside of the cell to the outside of the cell occurs through potassium selective “leak” channels that are expressed in high density (1, 8). As the  $K^+$  leaves the cells, negative charge builds up on the inner cell membrane as a result of the less permeable  $Cl^-$  ions that are not able to follow the  $K^+$  gradient. Active transport, through the  $Na^+/K^+$ -ATPase enzyme, for example, can work against the diffusion of  $K^+$  out of the cell by actively transporting two  $K^+$  into the cell for every three  $Na^+$  transported out. This bi-directional flow of  $K^+$  and, to a lesser degree other ions, is responsible for the negative resting potential in the cell (1, 8).

Changes in membrane potential can occur in response to the opening of voltage dependent ion channels (**Fig.3, top**), or other events including the binding of ligands to ligand gated channels. When these channels open they selectively pass ions through the membrane, which cause changes in the different ion populations across the membrane – also known as membrane potential. Sequential signaling of these proteins drives cyclical changes in the membrane potential, which is an important cellular signaling processes (1, 3, 26).

### Quantitative look at membrane potential

The energy stored in membrane potential results from the buildup of electrochemical gradients from three key ions: potassium, sodium, and chloride. Under steady state conditions, the cell membrane can be conceptualized as an RC (resistor capacitor) circuit with four parallel branches; one that represents the membrane dielectric properties (membrane capacitance ( $C_m$ ) and three branches, one for each key ion, which consists of a variable resistor and battery in series (1, 27). In this model ions, or current ( $I, I_x$ ), move through ion-selective channels which function as variable resistors ( $R_n$ ) with measurable conductance ( $g$ ),  $g = \frac{1}{R_n}$ . The difference

between internal and external concentrations for a particular ion species creates an ion specific potential difference ( $E_n$ ), which is represented as a battery.



Adapted from Hodgkin, A.L., and A.F. Huxley. 1952. *J. Phys.* 117: 500-544

The electrochemical gradients in the cell can be used to calculate membrane potential ( $V_m$ ) using multiple factors including: ion charge, concentration difference across the membrane and existing membrane potential ( $I, 3, 8$ ). The Nernst equation can be used to define the steady-state reversal potential ( $E_n$ ) for a given ion (n) with molar concentration  $[N]$  and ion valence ( $z$ ), at a given temperature ( $T$ , Kelvin) with the gas constant ( $R$ ) and Faraday constant ( $F$ , 23.062 kcal/V-mol):

$$E_n = \frac{RT}{zF} \ln \frac{[X]_{outside}}{[X]_{inside}}$$

Real cells exist under conditions of steady-state non-equilibrium with multiple ions. To address this, the Nernst equation can be expanded under the assumption that the membrane is semi-permeable, and the electric field is constant ( $I, 3, 8$ ). These assumptions give us the Goldman, Hodgkin and Katz equation, which is the sum of the Nernst equation for each key ion, weighted by the respective permeabilities ( $P_n$ ) of each ion:

$$V_m = \frac{RT}{F} \ln \frac{P_K [K^+]_{outside} + P_{Na} [Na^+]_{outside} + P_{Cl} [Cl^-]_{inside}}{P_K [K^+]_{inside} + P_{Na} [Na^+]_{inside} + P_{Cl} [Cl^-]_{outside}}$$

This equation can be rearranged to define permeability as a relative ratio between ions which is easier to measure experimentally:

$$V_m = \frac{RT}{F} \ln \frac{[K^+]_{outside} + \frac{P_{Na}}{P_K} [Na^+]_{outside} + \frac{P_{Cl}}{P_K} [Cl^-]_{inside}}{[K^+]_{inside} + \frac{P_{Na}}{P_K} [Na^+]_{inside} + \frac{P_{Cl}}{P_K} [Cl^-]_{outside}}$$

Using values provided by Hodgkin and Huxley,  $\frac{P_{Na}}{P_K} = 0.04$  and  $\frac{P_{Cl}}{P_K} = 0.45$ , the membrane

**TABLE 1: Typical intra/extracellular ion concentrations in neuron(27)**

| Ion[X]                    | [X]inside | [X]outside |
|---------------------------|-----------|------------|
| Potassium, K <sup>+</sup> | 400mM     | 20mM       |
| Sodium, Na <sup>+</sup>   | 50mM      | 440mM      |
| Chloride, Cl <sup>-</sup> | 51mM      | 560mM      |

potential at resting state – when ion channels are not opening in response to an external effector, can be estimated as -60mV(8, 27). At resting potential cells typically have a negative membrane potential. In physical terms this means the local field, which extends approximately 1nm from the cell membrane, has negative charge build up on the inside and a positive charge on the

outside of the cell. The changes in membrane potential are localized to the membrane of the cell, and proteins like the voltage sensing phosphatase detect and translate these changes into physiologically relevant phenomena.

### History of the voltage sensing domain

Voltage dependent proteins rely on a domain called the voltage sensing domain (VSD) to sense changes in membrane potential. Hodgkin and Huxley first predicted the presence of the voltage-sensing domain in their seminal 1952 paper describing a quantitative model for current in the giant squid axon.

*“...It seems difficult to escape the conclusion that the changes in ionic permeability depend on the movement of some component of the membrane which behaves as though it had a large charge or dipole moment.”(27)*

It was with these words that the field of voltage sensing was born, and twenty-one years later the gating particle that Hodgkin and Huxley referred to was identified when Armstrong and Bezanilla separated “gating current” from “ionic current”(28). The gating particle that Hodgkin and Huxley predicted was in fact the fourth helix of transmembrane protein domain that contained four helical transmembrane segments. S4, the fourth helical segment, contains an arginine rich motif, RXXRXXRXXR (R= Arg, X= any amino acid) (**Fig. 3**), which sits in the membrane and undergoes conformational changes in response to changes in the local charge at the membrane. These changes, which move the positive charge containing helix in response to the membrane field, produce a fast gating current ( $I_g$ ) that can be measured as a function of membrane voltage. The gating current tracks movement of the gating particle in the membrane, and precedes the ionic current ( $I_n$ ) that results from opening of the channel.

The gating model proposed by Hodgkin and Huxley assumed that the gating particle controlled conducting versus non-conducting states of the channel. This assumption can be approximated as a first-order kinetic model with  $y$  representing the probability of a conducting state,  $1 - y$  is the probability of the non-conducting state and the voltage dependent rate constants are  $\alpha_y(V_m)$  and  $\beta(V_m)$ :

$$(1 - y) \xrightleftharpoons[\beta_y(V_m)]{\alpha_y(V_m)} y$$

The probability of gate opening or closing during a short time increment is the product of the probability and the rate constant, and the rate of a single gating particle is the difference in these two probabilities:

$$\frac{dy}{dt} = \alpha_y(V_m)(1 - y) - \beta(V_m)y$$

With voltage clamped to a constant rate  $V_m$  over a longer time increment, the fraction of gates in the open state will become constant as a steady state is attained;  $t \rightarrow \infty$  and  $\frac{dy}{dt} \rightarrow 0$ . At steady state the conductance probability at  $V_m$  is:

$$y_{\infty}(V_m) = \frac{\alpha_y(V_m)}{\alpha(V_m) + \beta(V_m)}$$

From when the membrane potential is clamped to a given command voltage to when the system reaches steady state, the time course or kinetics of the process can be described as the solution to the first order kinetic expression, which is an exponential function where  $y_o$  is the value of  $y$  at holding potential, before the membrane potential is clamped to  $V_m$ :

$$y(t) = y_{\infty}(V_m) - (y_{\infty}(V_m) - y_o)e^{-t/\tau_y(V_m)}$$

The rate constant,  $\tau_y(V_m)$ , is defined as:

$$\tau_y(V_m) = \frac{1}{\alpha(V_m) + \beta(V_m)}$$

Bezánilla and Armstrong were able to record from cells containing gating particles and distinguish gating current from ionic current, but direct physical measurement of the gating particle would not occur for more than 20 years(28). Crystallizing membrane proteins was near impossible at the time, so in the mid-nineties several researchers developed creative chemical strategies for directly measuring S4 motion; Richard Horn used cysteine reactive probes to map the solvent accessibility of the S4 helix, and Ehud Isacoff tethered cysteine reactive environmentally sensitive probes to monitor motion of S4 (15, 29-32).

The approaches developed by Horn and Isacoff together with developments in crystallography, have led to a strong understanding of the VSD. When a cell is at rest, the inside of the membrane has a negative charge. Depolarization of the cell occurs when ions flow across the membrane, changing the negative charge on the inner surface of the cell membrane from net negative to net positive. The change in charge at the membrane is detected by the positively charged S4 helix, which ratchets out of the membrane in a helical motion, away from the more positively charged membranes inner leaflet and out of the cell(33-35).

### **The voltage sensing domain and VSP**

In 2005 a voltage sensing domain (VSD) was discovered in a non-conducting protein during sequence mining in the genome of the sea squirt *Ciona intestinalis*(7); the protein, a voltage sensing phosphatase (VSP), contained a voltage sensing domain that controlled the activity of a lipid phosphatase(36, 37). Until the discovery of the voltage sensing phosphatase, all known VSD containing proteins were ion channels with four VSDs arranged around an ion conducting pore domain; the four VSDs interacted cooperatively to “gate” the flow of ions through the pore domain(34, 38-41)In contrast, VSP contains a single monomeric voltage sensing domain that “gates” and enzyme (**Fig. 4**)(9). The discovery of VSP created a paradigm shift in the field of voltage sensing by demonstrating a previously unidentified modularity in the

VSD. This discovery also presented new challenges to researchers interested in studying the mechanistic coupling of the VSD, since the protein only had one VSD and thus carried a smaller total change, which resulted in a weaker gating charge signal that makes detection of gating current more challenging. Fortunately, voltage clamp fluorometry (VCF) proved to be a particularly effective tool for studying motions of the VSP voltage sensing domain.

In VCF a protein of interest is site specifically mutated to contain a cysteine (Cys) residue at the top of charge-containing S4 helix. RNA for this protein is injected into *Xenopus* oocytes, large cells that are up to 1.3mm in diameter(42). Over several days the oocytes express the protein on the plasma membrane. The cells are then exposed to external buffered solution containing environmentally sensitive dyes that have been modified to contain a maleimide. The maleimide reacts with the Cys and covalently tethers the dye to the top of S4. The cell is then used in two electrode voltage clamp experiments, where the cell can be clamped from a resting membrane potential ( $V_{rest}$ ) to a defined holding potential ( $V_{hold}$ ) based on commands outlined in a protocol(30). The environmentally sensitive fluorophore moves from a set of solution conditions that are a function of the  $V_{rest}$  state, to another set of solution conditions that are a function of the  $V_{hold}$  state (**Fig.5a**). The changes in fluorophore quenching in response to the protocol can be monitored and compared between different protein mutants(10, 21, 30, 43-47). Since the S4 helix ratchets out of the membrane, the quenching events or de-quenching events on the probe report on the macroscopic S4 motions through distinct states(9, 10, 26, 33, 40, 41, 43, 44, 46-53).

One labeling site (G214C) at the top of S4 in the VSD of Ci-VSP reports a decrease in fluorescence, or quenching, in response to changes in membrane potential that fits the model of gating proposed by Hodgkin and Huxley (**Fig.5b**)(27). The fluorescence readout has distinct *ON*, *STEADY STATE* and *OFF* kinetics (**Fig.5c**). The steady state change in fluorescence can be plotted against voltage, and fit with a Boltzmann sigmoid, which is consistent with Hodgkin and Huxley first order kinetic approximation for steady state gating particle movement (**Fig.5d**):

$$y_{\infty}(V_m) = \frac{\alpha_y(V_m)}{\alpha(V_m) + \beta(V_m)}$$

The *ON* and *OFF* kinetics of the fluorescence traces exhibit bi-exponential behavior with voltage dependent rate constants ( $\tau_{fast}$  and  $\tau_{slow}$ ) and amplitudes ( $A_{fast}$  and  $A_{slow}$ ) (**Fig.6a-c**):

$$y(t) = A_f(V_m)e^{-t/\tau_{fast}(V_m)} + A_s(V_m)e^{-t/\tau_{slow}(V_m)}$$

The fast rate constant  $\tau_{fast}$ , matched the rate constant of gating charge motion(47) (**Fig.6d**) suggesting that the environmentally sensitive probe monitored structural changes that occurred in the same region and at the same time scale as gating charge motion:

$$\tau_y(V_m) = \frac{1}{\alpha(V_m) + \beta(V_m)}$$

Since VCF monitors changes in the VSD with high precision, it is a powerful tool for monitoring structural and conformational changes in the protein. To characterize allosteric coupling between the voltage sensing domain (VSD) and the phosphatase domain, voltage dependent

conformational changes monitored by VCF are correlating with corresponding voltage dependent changes in the activity and specificity of the phosphatase domain.

## CHEMICAL CHANGES IN THE CELL

### PIPs and the potential function of VSPs

Electrochemical changes in membrane potential are transduced into chemical changes by VSP, which upon activation de-phosphorylates the head group on phosphatidylinositol-phosphate signaling lipids (PIPs). PIPs control a vast number of important tasks in the cell through binding events at the membrane-cytosol interface. PIPs bind to proteins and effectors at the cell membrane to regulate and induce changes in the cell adhesion, motility, signal transduction and endo/exocytosis among others(20, 23, 54, 55). PIPs also regulate ion channels and transporters through binding to membrane domains(26, 56, 57).

### Overview of protein tyrosine phosphatases

VSP is a dual-specificity protein tyrosine phosphatase, and thus functions as a lipid phosphatase instead of as a classic protein tyrosine phosphatase. All members of the PTP family have the conserved HCXXGXXR active site motif (X means any residue)(22, 24, 58, 59). In the general PTP enzyme mechanism the active site cysteine attacks the target phosphate through nucleophilic attack(24, 60, 61). The catalytic function for VSP is most similar to PTEN, another dual-specificity protein tyrosine phosphatase that functions as a lipid phosphatase(20, 21). In contrast to VSP, PTEN is entirely cytosolic with a short N-terminal lipid-binding region that regulates association with the membrane(29). PTEN and VSP share 44% homology, but PTEN acts very specifically as a 3-position phosphatase, while VSP exhibits broader specificity(7). VSP and PTEN both work on phosphorylated versions of phosphatidylinositol (PIPs). Due to their importance, mutations in PIP phosphatases are implicated in many diseases including cancer, down syndrome, asthma and cancer(57, 62-64).

### Phosphatase domain and linker in VSP

Conformational changes in the VSD occur in response to changes in membrane potential and these changes result in activation of a lipid phosphatase domain (PD) in VSP. Several previous groups have shown that VSP is a 5-position lipid phosphatase. VSP acts on the inositol ring of phosphorylated phosphatidylinositol lipids (PIPs), converting PI(4,5)P<sub>2</sub> to PI(4)P and PI(3,4,5)P<sub>3</sub> to PI(3,4)P<sub>2</sub>(7).

VSP is homologous to PTEN, a cytosolic lipid phosphatase that is part of the protein tyrosine phosphatase (PTP) superfamily. PTEN and VSP share strong homology, particularly between the phospholipid-binding motif (PMB) in PTEN and the 16 amino-acid long linker that connects the VSD to the PD in VSP. The importance of this region has been demonstrated in multiple studies(7, 10, 52). Since PTEN does not have a VSD and is completely cytosolic, it relies on the PBM to access to substrate and localization to the membrane(29, 31, 32, 59). When arginine residues in the linker are mutated to any other residue PTEN cannot associate with the membrane, a similar result is also seen when arginines in the linker are neutralized(52). It has been shown that the linker conveys information between the enzyme active site and the voltage-sensing domain(10), but what remains to be understood is the extent of regulation the VSD has over the enzyme active site.

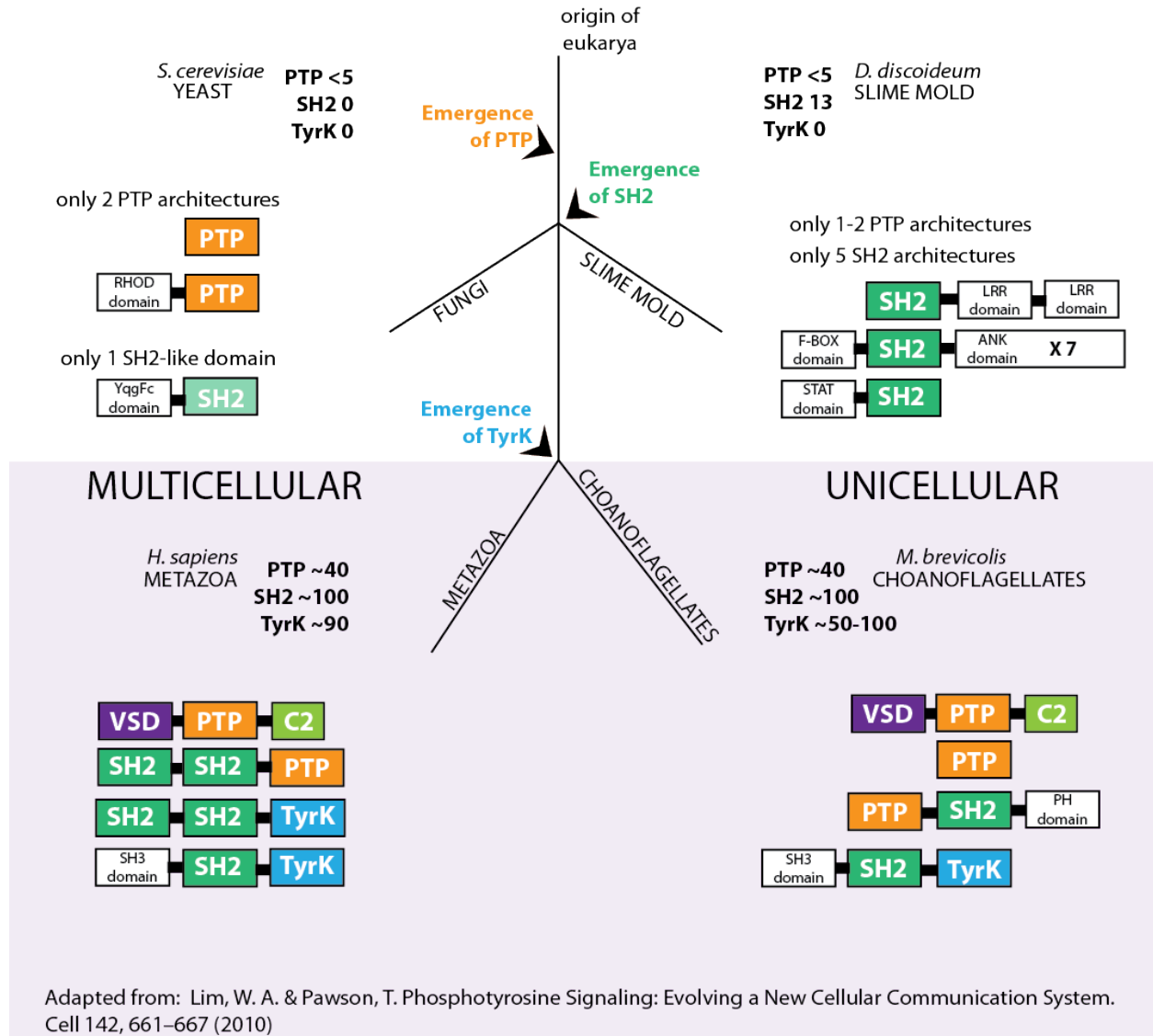
In this work several important questions about inter-domain coupling between the VSD and the PD are addressed. Specifically, the aim is to understand the allosteric coupling and regulation imposed by the VSD on the PD. Correlating voltage dependent conformational changes in the VSD reported by VCF with a new tool developed for monitoring VSP enzyme



specificity, this work expands on the existing understanding of allostery by showing that a distant effector domain can regulate active domain specificity.

The data presented in this dissertation suggests that inter-domain coupling between unrelated multistate domains can evolve tight allosteric control, with distinct states in the effector domain exerting direct control over multiple states in the active domain. This principle, which demonstrates that multi-state effector domain can exert control of multiple states in an active domain, may be generalizable and could translate to other systems that have not yet been explored in this context. Furthermore, understanding the mechanism of voltage sensing and inter-domain coupling in this novel protein also provide insight that can be applied to engineer new proteins(6)including new novel voltage sensing enzymes(65), and high fidelity, fast reporters for optically monitor changes in membrane potential(66-68).

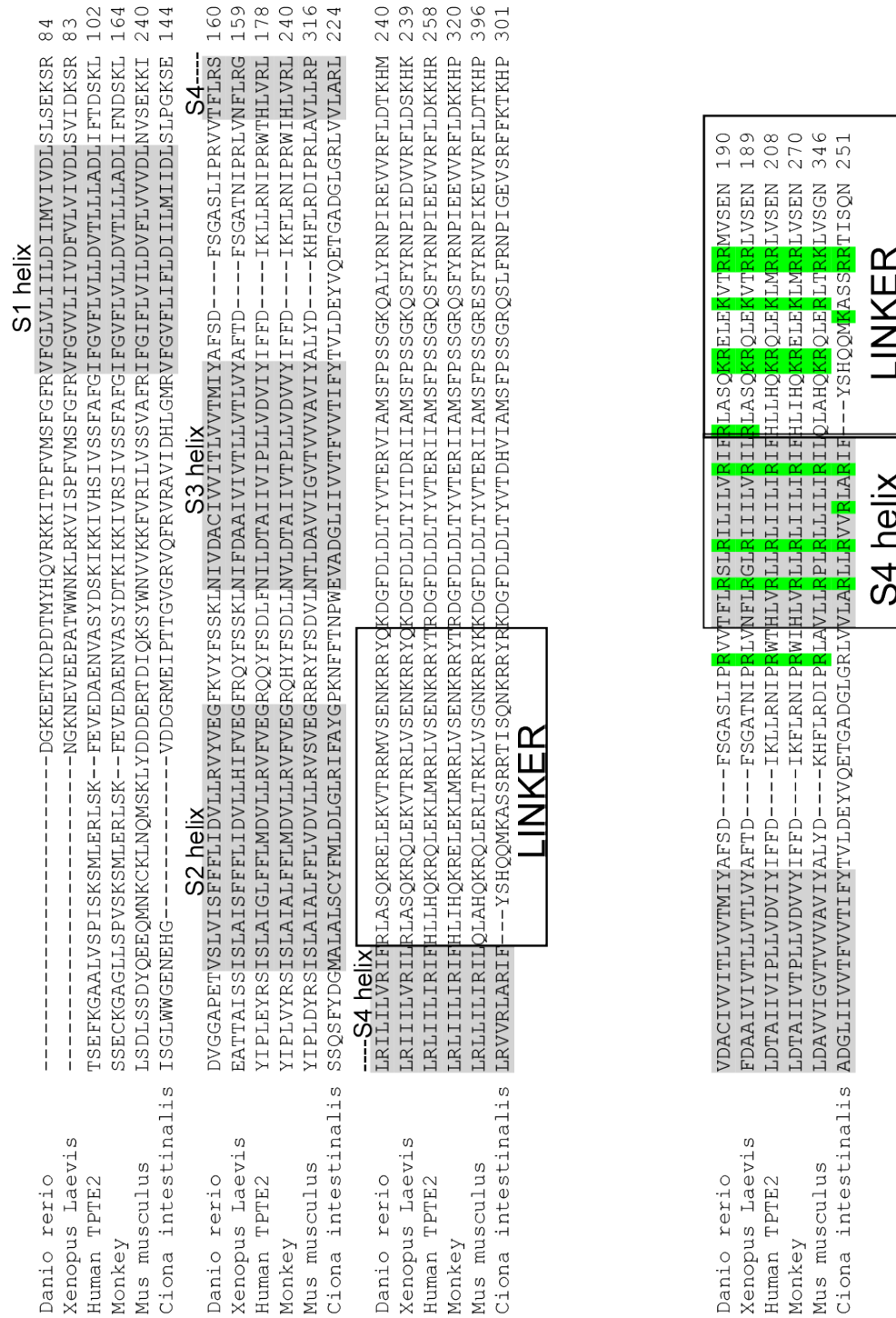
## FIGURES



### Figure1. Protein Domains and Evolution.

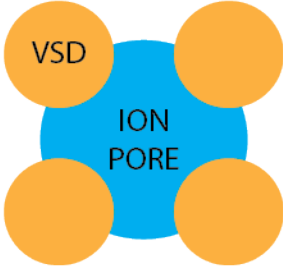




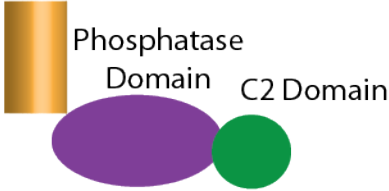
Schematic representing the evolution of sophisticated domain architecture in protein tyrosine phosphatase (PTP), tyrosine kinase (TyrK) and SH2 containing proteins. Yeast and slime mold contain very few proteins with PTP or SH2 domains, and no proteins with combinations of PTP/SH2 domains. The choanoflagellate and metazoan genomes contain far greater numbers of PTP/SH2/TyrK proteins, and have more sophisticated domain architecture with combinations of the different domains. Similarly, VSP which contains a PTP domain, is not found in yeast and slime mold, but is found in choanoflagellates and metazoan.





**Figure3. Sequence alignment of VSD across species.**

The VSD consists of four transmembrane helices, S1-S4, with the fourth helix (S4) containing positively charged Arg (green) that sense and respond to changes in membrane potential. The linker also contains many basic residues that bind to the head groups of PI(4,5)P<sub>2</sub> in the membrane.

| PROTEIN FAMILY   | DOMAIN ARCHITECTURE   | PROTEIN FUNCTION                        |
|--|---|---|
| V-dependent ion channels<br>            | four VSDs around a pore domain<br>                 | conducts ions                           |
| V-dependent H <sup>+</sup> channels<br> | two VSDs<br>                                       | conducts protons                        |
| Voltage Sensing Phosphatase<br>       | one VSDs<br>Phosphatase Domain<br>C2 Domain<br> | removes phosphate from signaling lipids |

**Figure4. Domain architecture of VSD-containing proteins.**

VSD containing proteins can be divided into three classes based on the number of VSDs they contain. Voltage dependent ion channels (**Fig.4, top**) contain four VSDs assembled around a functional pore domain, which conducts ions. The voltage dependent proton channel (**Fig.4, middle**) consists of two voltage sensing domains dimerized through a coiled-coil domain; each of the VSDs conducts protons in response to changes in membrane potential. The voltage sensing phosphatase proteins (VSPs) (**Fig.4, bottom**) differs significantly from the other two VSD containing proteins, it contain one single VSD that gates the cytosolic phosphatase domain enabling the enzyme to become active in response to changes in membrane potential.

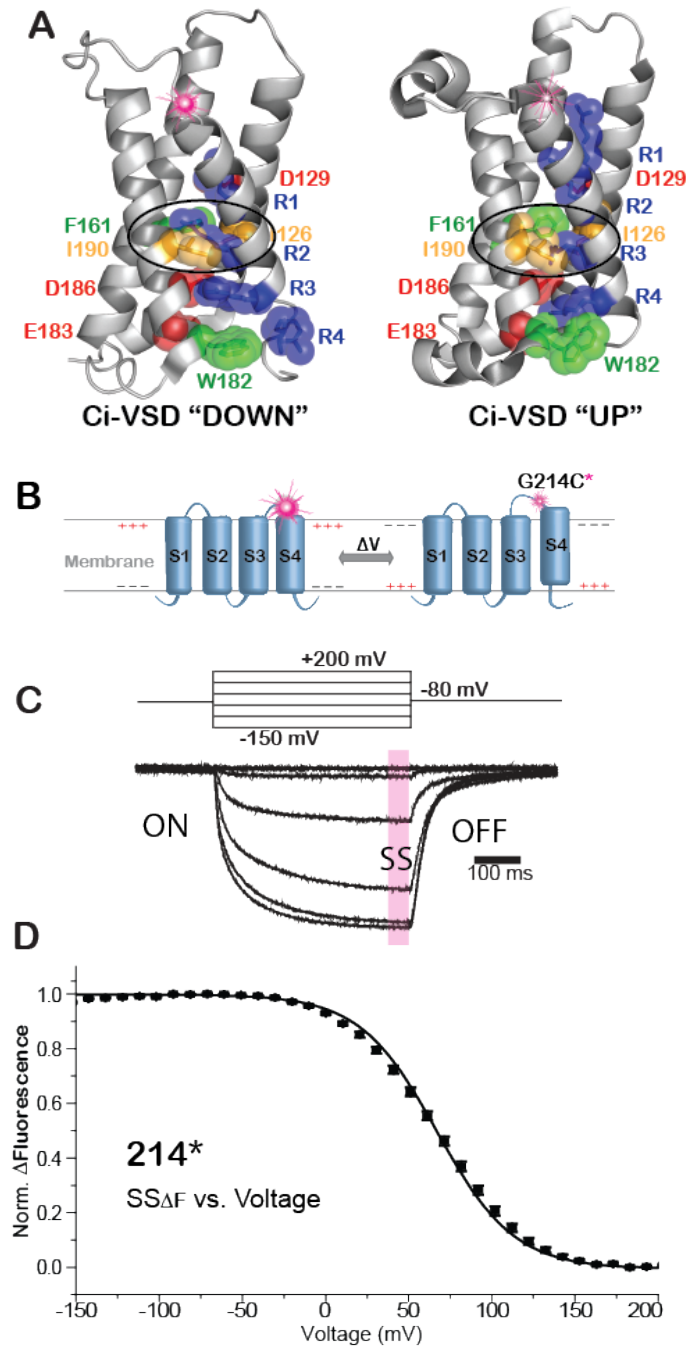


### Figure 5. VCF reports changes in the VSD

The voltage sensing domain moves from an *OFF* to an *ON* state in response to changes in membrane potential (Fig. 5A). An environmentally sensitive probe can be covalently attached to a Cys site specifically introduced to the top of S4 (Fig. 5B). The probe quenches in response to changes in membrane potential (Fig. 5C). A plot of the steady-state change in fluorescence (Fig. 5C, pink) for the fluorophore at a range of voltages is fit well by a single sigmoid (Fig. 5D).

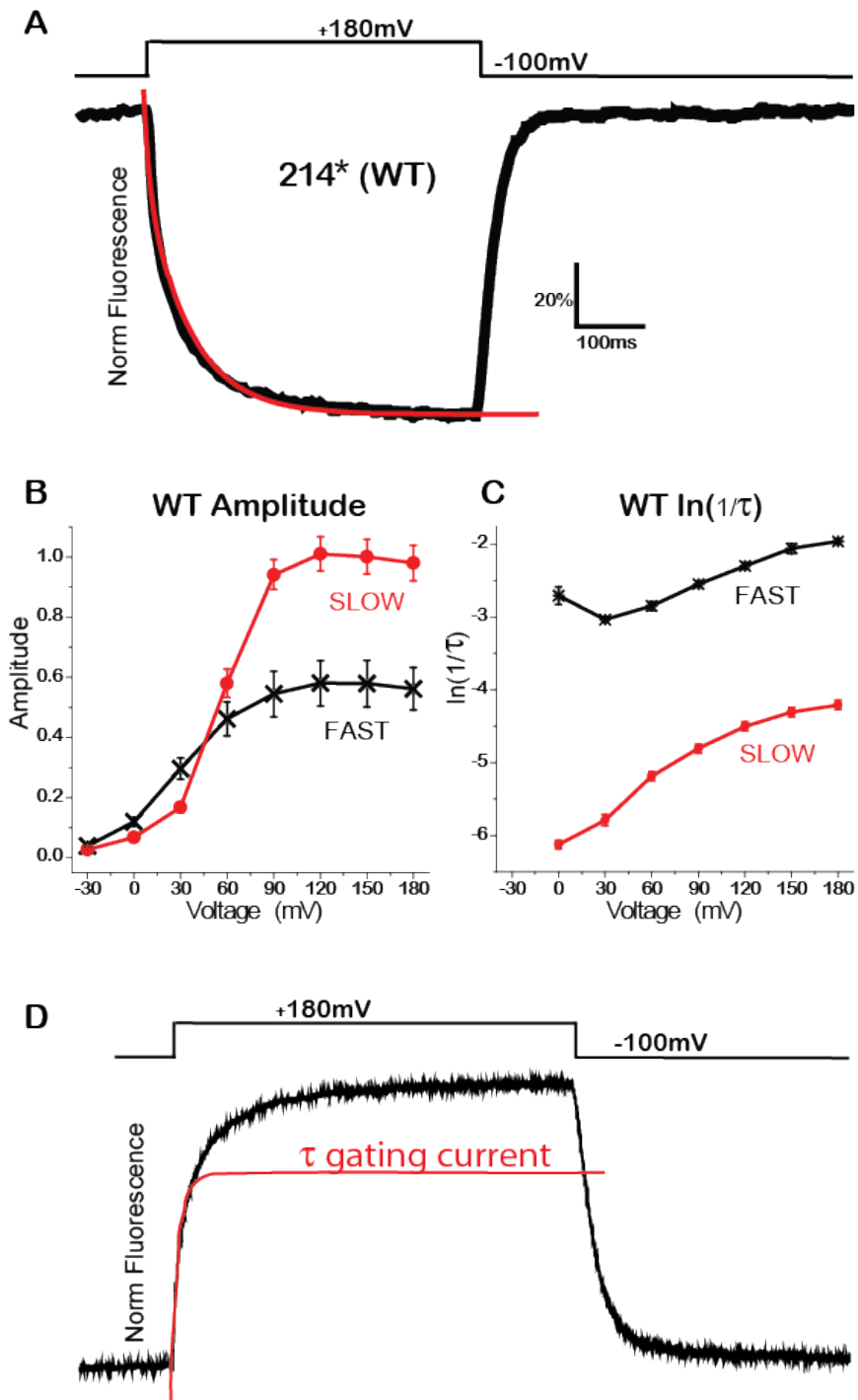


**Figure 6. Kinetics of 214\* show properties of Hodgkin and Huxley gating particle**  
 The ON kinetics of the 214\* fluorescence response can be fit by a double exponential (Fig.6A) with amplitudes (Fig.6B) and rate constants (Fig.6C) that are voltage dependent. The gating charge rate constant matches the rate constant of the fast component of fluorescence (47) (Fig.6D). These features are consistent with the model of the gating particle proposed by Hodgkin and Huxley(27).

## ALLOSTERIC SUBSTRATE SWITCHING IN VOLTAGE SENSING PHOSPHATASE

### ABSTRACT:

Phosphoinositol phosphate signaling lipids (PIPs) are important second messengers that regulate ion channels, transporters, cell motility and endo/exocytosis. PIP concentrations are controlled by enzymes, including the voltage sensing phosphatase (VSP), which has broad specificity for a diverse class of PIPs. VSP is a novel lipid phosphatase, which contains a voltage sensing domain (VSD) homologous to voltage-gated ion channels, and a lipid phosphatase domain (PD). Until now it was not known what properties of the cytosolic PD were allosterically regulated by the membrane-associated VSD. We developed fast PIP sensors to monitor enzyme activity and using voltage clamp fluorometry to monitor conformational changes in the VSD, find that the *Ciona intestinalis* VSP (Ci-VSP) has two distinct voltage regulated enzyme active states: a faster low-voltage state with substrate preference for PIP<sub>3</sub> and a slower high-voltage state with preference for PIP<sub>2</sub>. This novel 2-step allosteric switch for enzyme specificity enables membrane potential to function as an allosteric effector that dynamically regulates PIP concentration.



## INTRODUCTION:

The concepts of allostery are constantly evolving with the discovery of new proteins and experimental advancement(69). Allostery is a critical mechanism for regulation of enzymes and, by extension signaling pathways that involves phenomenological control over an enzyme active site through binding of another metabolite at a ‘non-overlapping’ allosteric site(70-72). In the systems described to date, allosteric regulation has been found to regulate an enzyme preference on a single preferred substrate(73). Here we expand the existing understanding of allostery by demonstrating that a distant effector domain can regulate substrate specificity in an attached active domain.

Voltage sensing phosphatases (VSPs) are membrane-associated enzymes that dephosphorylate phosphatidylinositol signaling lipids in response to changes in membrane potential, thereby enabling the electrical activity of a cell to couple to intracellular signaling pathways(57, 74). VSP is found in all animals, but the most studied and first characterized VSP is Ci-VSP – the VSP derived from the sea squirt *Ciona intestinalis*(7). VSPs consist of two domains; a transmembrane voltage sensing domain (VSD) and a cytosolic phosphatase domain (PD). The VSD is homologous to the VSD of voltage sensing ion channels – it consists of four transmembrane helices with a characteristic voltage sensing S4 segment that contains four arginine residues. The PD of VSP is homologous to the lipid phosphatase PTEN, a tumor suppressor protein that is recruited to the membrane through a PI(4,5)P<sub>2</sub> specific binding motif (PBM). The PBM of PTEN shares strong sequence conservation with the 16 amino-acid linker that connects the transmembrane VSD and cytosolic PD of VSPs(31, 59, 75); in Ci-VSP this region couples VSD responses to membrane depolarization with activation of the PD (10, 47, 52).

Although the PD of Ci-VSP resembles PTEN structurally, the two enzymes exhibit different substrate preferences. PTEN hydrolyzes phosphates from the 3-position of PI(3,4,5)P<sub>3</sub> and PI(3,4)P<sub>2</sub> substrate; however, Ci-VSP can remove both 3-phosphate from PI(3,4,5)P<sub>3</sub> and PI(3,4)P<sub>2</sub> and 5-phosphate from PI(3,4,5)P<sub>3</sub> and PI(4,5)P<sub>2</sub>.(32, 75, 76) Attempts to introduce PTEN specificity for 3-phosphate into VSP based on homology models to generate active site mutations have had only partial success, (21, 77) suggesting that additional factors play a role in the difference between the enzymes. An apparent separation in voltage dependence between the production and destruction of PIP<sub>2</sub> by VSP was observed earlier, but it was not clear whether this reflected a property of voltage regulation or a bias on substrate binding based on substrate charge (20).

Studies on voltage-gated K<sup>+</sup> channels and Ci-VSP have established that membrane depolarization drives VSDs to transition between multiple conformations(9, 10, 33, 40, 41, 43, 44, 46-53). This led us to ask if distinct conformations in the VSD may place the PD into distinct active states, each with its own substrate specificity.

A limitation in the earlier studies was the use of soluble fluorescent PIP reporters that slowly partition between the cytoplasm and plasma membrane as membrane PIP concentrations change, introducing kinetic delay and constraining the number of measurements that could be made in each cell, thereby hampering the determination of the voltage dependence of activity. To overcome these problems, we generated two new fast genetically-encoded fluorescent reporters, one for PI(3,4)P<sub>2</sub> and another for PI(4,5)P<sub>2</sub>, based on an earlier design that permanently targets the reporter to the membrane and reads out PIP binding as a change in FRET (58). These new reporters have vastly faster kinetics and improved reproducibility. We complemented these reporters of enzyme activity with voltage clamp fluorometry (VCF) to measure the kinetics and

voltage dependence of conformational changes in the VSD(2, 9, 10). We find that small depolarizations in wildtype Ci-VSP produce accumulation of both PI(3,4)P<sub>2</sub> and PI(4,5)P<sub>2</sub> and that large depolarizations evoke a transient accumulation of these PIP<sub>2</sub> species followed by their depletion. Strikingly, VSD mutations that stabilize an intermediate VSD conformation enhance PIP<sub>3</sub>→PIP<sub>2</sub> catalysis and strongly dampen PIP<sub>2</sub>→PIP catalysis, whereas a mutation that stabilizes the state to which the VSD is driven by strong depolarization enhances PIP<sub>2</sub>→PIP catalysis. Thus, sequential transitions between three conformations of the VSD are coupled to transitions between three functional states of the PD: an inactive state at negative voltage to the PIP<sub>3</sub>-preferring state at intermediate voltage and then to the PIP<sub>2</sub>-preferring at strong depolarization. This intriguing mechanism of substrate switching enables the enzyme to operate in two distinct modes at different voltages as well as to produce complex temporal patterns of PIP signaling. The ability of a single allosteric domain to control entry into more than one active state by virtue of its ability to assume multiple conformations, and, indeed, to enable sequential transitions between them, provides a logic by which enzymes may achieve complex operations.

## RESULTS

### New fast PIP<sub>2</sub> reporters

To measure the voltage dependence of Ci-VSP phosphatase activity, we needed a fast reporter of changes in PIP<sub>2</sub> concentration that would enable kinetic analysis and sampling of activity across a broad voltage range. The original class of soluble fluorescent protein-tagged PH (pleckstrin homology) domain protein reporters (4, 5, 20, 21, 76, 78) proved difficult to use because of their slow partitioning between the cytosol and the plasma membrane (**Supplementary Fig. 1a**). The long settling times posed several problems: a) they required long voltage steps (~60 seconds), which led to substantial PIP depletion and required long recovery periods between voltage steps, limiting the resolution and voltage range that could be examined, b) they resulted in substantial photobleaching of the fluorescent protein tag, and c) they blurred kinetically distinct components.

A membrane-tethered reporter should respond to changes in PIP concentration more quickly by avoiding the slow equilibration between cytosol and plasma membrane. Such a reporter would need to detect PIP binding not by re-localization but by another means. We turned to the CFP/YFP-based Förster Resonance Energy Transfer (FRET) reporter “Fllip-pm,” which is permanently targeted to the plasma membrane through CAAX prenylation and contains a PH domain from GRP1, which binds PI(3,4,5)P<sub>3</sub> (6, 58) (**Fig. 1a, Supplementary Fig. 1b**). We replaced the specificity determining regions of GRP1 PH domain with that of either TAPP1 or PLC1δ, which selectively bind either PI(3,4)P<sub>2</sub> or PI(4,5)P<sub>2</sub>, respectively, to make “F-TAPP” and “F-PLC.” F-TAPP and F-PLC had much shorter delays and faster fluorescence changes in response to activation of Ci-VSP by a voltage jump, than did cytosolic versions of the reporters (**Supplementary Fig. 1c,d**).

### Wildtype Ci-VSP appears to transition sequentially between two distinct enzymatic states

Wildtype Ci-VSP was co-expressed with either F-PLC or F-TAPP (**Fig. 1a**). Each cell was depolarized from a holding potential of -100 mV, where the enzyme is inactive, to one of a series of command voltages for 2 seconds before returning to -100 mV for a 45 sec rest before the next voltage step. Using this protocol, we set out to determine whether membrane depolarization simply activates the enzyme or if it also modulates substrate selectivity (**Fig. 1b**).

For F-PLC, depolarizing steps to +30mV and higher evoked a small, transient increase in FRET, which reached a maximum at about +90 mV (**Fig. 1c, inset**). Beginning with steps to about +60 mV, the initial increase in FRET was followed by a large decrease (**Fig. 1c**). The two-phase behavior suggests that VSP first dephosphorylates PI(3,4,5)P<sub>3</sub> at the 3-position to produce PI(4,5)P<sub>2</sub> and then dephosphorylates PI(4,5)P<sub>2</sub> at the 5-position to produce PI(4)P (**Fig. 1b,d**).

For F-TAPP, depolarizing steps to 0mV and higher evoked an increase in FRET, which reached a maximum at about +30 mV (**Fig. 1e**). Beginning with steps to about +60 mV, the initial increase in FRET was followed by a decrease (**Fig. 1e**). This behavior suggests that VSP first dephosphorylates PI(3,4,5)P<sub>3</sub> at the 5-position to produce PI(3,4)P<sub>2</sub>, and then dephosphorylates PI(3,4)P<sub>2</sub> at the 3-position to produce PI(4)P (**Fig. 1b,d**).

Together, the F-PLC and F-TAPP data suggest a model whereby membrane depolarization from an initial negative voltage sequentially drives VSP from an inactive state into one active state and then another, with these active states consisting of an early PIP<sub>3</sub>-preferring state (A1) and a later PIP<sub>2</sub>-preferring state (A2), with both states able to dephosphorylate at either the 5-position or 3-position (**Fig. 1f**). The observation that the early rise in FRET for both reporters reaches a maximum at voltages beyond which the late decline in

FRET continues (**Fig. 1c,e**), suggests that A1 may be favored at low depolarization and A2 at high depolarization. However, the voltage range over which these occur clearly overlap considerably in wildtype CiVSP. We therefore set out to test this model by dissecting apart the two active states.

### Sequential conformational changes in the VSD and state-stabilizing mutants

To test the notion that depolarization turns Ci-VSP on in two phases of distinct phosphatase activity, first to a PIP<sub>3</sub>-preferring A1 state that is favored at intermediate voltages and then to a PIP<sub>2</sub>-preferring A2 state that is favored at more positive voltages, we set out to better resolve these states. Our goal was to identify a conformational sequence in the VSD that is associated with the transitions in the PD and then make mutations to the VSD that stabilize it in the intermediate or fully activated state in an effort to preferentially stabilize either A1 or A2.

We began with a cysteine substitution at residue 214 in the S3-S4 loop (G214C), which we used as an attachment site for the environmentally-sensitive fluorophore tetramethyl-6-rhodamine-maleamide (TMRM) (**Fig. 2a**). TMRM has been used extensively to detect voltage-driven conformational changes in VSDs (*9, 10, 30, 33, 45, 79-81*) including at the 214C position in Ci-VSP (*9-11, 21*). Depolarization evokes a two-step  $\Delta F$  from 214C-TMRM, consisting of fast and slow components (**Fig. 2b**) (*10, 12, 47, 52*). The steady-state fluorescence-voltage relation (F-V) is well fit by a single Boltzmann relation (**Fig. 2c, black symbols and curve**).

In effort to stabilize discrete conformations of the VSD, we considered that, in ion channels, as S4 moves outward in response to membrane depolarization its arginines ratchet between electrostatic interactions with acidic partners and cross barriers made of bulky hydrophobic side chains (*13, 14, 32, 33, 49, 75, 76, 82-87*). Increasing the bulk of the hydrophobic side chains can increase the barrier to S4 motion, as can substitution of an arginine side chain by a longer lysine side chain (*17, 21, 77, 78, 83, 88-94*). Ci-VSP has two potential hydrophobic barriers that face the arginines of S4, one near the middle of the membrane formed by I126, F161 and I190 and the other at the internal end of S4 formed by W182 (*95*) (**Fig. 2d**). In an attempt to stabilize an intermediate conformation of the VSD, we sought to obstruct the outward motion of S4 by substituting the phenylalanine of 161 with a bulkier tryptophan (F161W) and by individually replacing with lysine the arginines that appear to cross this middle barrier: R226K (R2K) and R229K (R3K), as well as the one that crosses the internal barrier R232K (R4K).

The F-V of R2K and R3K were well-fit by a single Boltzmann, similar to wildtype (**Fig. 2e, f blue**). However, the F-V of F161W and of R4K were each separated into two components, with midpoints that differed by  $80 \pm 13$  mV in F161W, and  $91 \pm 10$  mV for R4K (**Fig. 2c,g**). Even so, there remained considerable overlap between the two components in these single mutants. We therefore combined F161W with each of the R $\rightarrow$ K mutants. The addition of R3K to F161W (F161W/R3K) increased the separation to  $113 \pm 6.6$  mV (**Fig. 2f**), but the most promising combination, F161W/R4K, in which the individual mutants each produced a large separation, had only a single component (**Fig. 2g**). Because the single component of F161W/R4K had the voltage dependence of the more negative component of R4K (**Fig. 2g**), we wondered whether the intermediate had been so stabilized that the second component was shifted out of the range of our test voltages. To address this, we turned to another fluorophore attachment site that is farther out in the S3-S4 loop, Q208C (**Fig. 3a**).

As shown earlier (*10, 16*), Q208C-TMRM has a triphasic  $\Delta F$ , indicating three conformational changes. There is a small and fast increase in fluorescence between -100 and 0 mV (F1), where we find the enzyme to be inactive, and there are two fluorescent components

over the voltage range where the enzyme is active: i) an intermediate speed fluorescence decrease between about 0 and +90 mV (F2), and a late slow fluorescence increase at more positive voltages (F3) (**Fig. 3b, c**). The F161W/R3K double mutant appeared to shift F2 in the positive direction to overlap with F3 (**Fig. 3d, e**). However, the F161W/R4K mutant strongly suppressed the amplitude of F3 with minimal effect on F1 and F2 (**Fig. 3f, g**), showing that the F161W/R4K mutation does indeed stabilize an intermediate activated conformation of the VSD.

To favor full activation, we attempted to eliminate a barrier to outward S4 motion. We focused on an inner hydrophobic residue, W182, which we substituted with a much smaller alanine (W182A). The W182A mutation shifted both F2 and F3 in the negative direction (**Fig. 3h,i**), consistent with the reduction of a barrier to activation and rendering easier entry into the fully activated conformation of the VSD.

Having made mutants that appear to stabilize the intermediate state of the VSD (F161W/R4K) or ease its entry into the fully activated state (W182A), we returned to our FRET reporter assays to analyze the effects of these mutations on activity.

### **VSD mutants favor A1 or A2 state of the PD**

To test the effect on enzyme activity of mutants that stabilize distinct states of the VSD, we used F-TAPP and F-PLC to monitor the voltage-triggered production and consumption of PI(3,4)P<sub>2</sub> and PI(4,5)P<sub>2</sub>, respectively. We first tested the F161W/R4K double mutant, which stabilized the intermediate activated conformation of the VSD. Using the F-TAPP reporter to track PI(3,4)P<sub>2</sub>, we found that the early phase of fluorescence increase seen with WT Ci-VSP (**Fig. 1e and d, open symbols**) was preserved in the F161W/R4K double mutant (**Fig. 4a,b**), but that the late phase of fluorescence decrease was eliminated (**Fig. 4b and c, open symbols**). Using the F-PLC reporter to track PI(4,5)P<sub>2</sub>, we found that the small early phase of fluorescence increase seen with WT Ci-VSP (**Fig. 4c**) was preserved in the F161W/R4K double mutant, but that the large late phase of fluorescence decrease was severely attenuated (**Fig. 4a and c, closed symbols**). These observations suggest that F161W/R4K has a relatively normal PIP<sub>3</sub> dephosphorylating A1 state, but is blocked from entry into the PIP<sub>2</sub> dephosphorylating A2 state, even at strong depolarization. This finding is consistent with the impact of the F161W/R4K double mutant on VSD motion as reported by 208C-TMRM, as seen above, which was to allow entry into the intermediate activated state, but suppress entry into the fully activated state (**Fig. 3g**).

We next turned to W182 at the internal hydrophobic plug, which R4 crosses when S4 moves outward during activation (*14, 18, 95*) (**Fig. 2d**), and whose mutation to alanine (W182A) we found to shift to more negative voltages entry into both the intermediate and fully activated conformations of the VSD (**Fig. 3i, Supplementary Fig. 5c**). Using the F-TAPP reporter to track PI(3,4)P<sub>2</sub>, we found that the early phase of fluorescence increase seen with WT Ci-VSP (**Fig. 1e**) was observed at more negative voltages in the W182A mutant, and that the late phase of fluorescence decrease also was detected at more negative voltages and, indeed, became large enough and fast enough at strong depolarization to blunt the amplitude of the early phase of fluorescence increase (**Fig. 4f and g, open symbols**). Similarly, using the F-PLC reporter to track PI(4,5)P<sub>2</sub>, we found that the small early phase of fluorescence increase seen with WT Ci-VSP (**Fig. 1c, inset**) was reduced in amplitude in the W182A mutant (**Fig. 4e, inset**), and that the large late phase of fluorescence decrease was shifted to more negative voltages (**Fig. 4e and g, closed symbols**).

Thus, our observations indicate that a double mutation in the VSD, which prevents entry into the fully activated conformation of the VSD, prevents entry of the PD into the PIP<sub>2</sub> dephosphorylating A2 state and limits Ci-VSP to operate almost entirely in the A1 state, as a

PIP<sub>3</sub> dephosphorylating enzyme. In contrast, a mutation in the VSD that eases entry into the fully activated conformation of the VSD favors operation of the PD in the A2 state as a PIP<sub>2</sub> dephosphorylating enzyme.

### **VSD conformations in inactive and active states of PD**

The recent crystal structures of the isolated VSD from Ci-VSP revealed two conformations: one of the wildtype protein, whose VSD is favored to be at rest under the zero voltage conditions of crystallization, and the other from a point mutant to glutamate of an arginine at the outer end of S4 (R217E) (**Fig. 2d**), which shifts the voltage dependence of gating charge motion in the negative direction so that the VSD is favored to be activated at zero voltage(16, 22, 95).

We first asked which VSD conformation seen in our fluorescence measurement from Q208C-TMRM is reached at zero voltage in the R217E mutant. We found that the F-V was shifted in the negative direction, as expected, and that the intermediate activated state, in the trough between F2 and F3, is occupied at zero voltage (**Fig. 5b**). We next asked which activity state is reached in R217E at zero voltage. Using the F-TAPP reporter to track the production and dephosphorylation of PI(3,4)P<sub>2</sub>, we found that the R217E mutation shifts the voltage dependence of activity in the negative direction, again as expected, and that zero voltage corresponds to the voltage with the maximal increase in PI(3,4)P<sub>2</sub> (**Fig. 5c,d**). These results indicate that the “up” conformation of the VSD seen in the Ci-VSP R217E crystal structure corresponds to the A1 activity state of the PD.

## DISCUSSION

Using new, fast reporters of two species of PIP<sub>2</sub> that we generated to monitor lipid phosphatase enzyme activity, we find that Ci-VSP has two distinct activity states: a low-voltage state, A1, with substrate preference for PIP<sub>3</sub>, and a high-voltage state, A2, with preference for PIP<sub>2</sub>. In wildtype Ci-VSP, high voltage steps elicit sequential transition from the inactive state at negative voltage first into the A1 state and then into the A2 state. Since the VSD undergoes a series of conformational changes in response to membrane depolarization (refs), we made mutations that were designed to stabilize the VSD in different conformations by increasing or decreasing barriers for the outward motion of S4. Voltage clamp fluorometry measurement of the conformational changes in the VSD identified two mutants that stabilize different VSD conformations. One of these (F161W/R4K), which we designed to increase the barrier to outward S4 motion both by increasing the bulk of hydrophobic plug residue 161 from a phenylalanine to a tryptophan and by substituting S4's fourth arginine with the longer lysine, stabilized an intermediate conformation of the VSD. The other (W182A), which we designed reduce the barrier to S4 motion by substituting S4-facing tryptophan 182 with a much smaller alanine stabilized the fully activated conformation. We find that the first mutant allows the enzyme to activate to the A1 state, but almost eliminates its ability to enter the A2 state, consistent with the observed strong stabilization of the intermediate activated conformation of the VSD. Moreover, we find that the second mutant eases entry into the A2 state, as predicted from the easier full activation of the VSD.

While our voltage clamp fluorometry measurements reveal multiple conformational transitions in the VSD of the protein, crystal structures have been obtained for only two conformations, which differ by only “one click” (i.e. where S4 has moved outward so that the arginines are displaced by one register)(23, 95). One of the structures was of the wildtype Ci-VSP, whose VSD is favored to be at rest due to the absence of a membrane electric field, and the other was of the R217E mutant, which shifts the voltage dependence of gating charge displacement so that the VSD is favored to be activated at zero voltage. While the wildtype Ci-VSP is inactive at zero voltage, we found that the R217E mutant is in the A1 state at zero voltage (Fig. 5e). This suggests that the VSD undergoes one more rearrangement, possibly a “second click,” to drive the PD into the A2 state.

Our finding that Ci-VSP has two different active enzyme states provides a precedent that may apply to other enzymes as well, perhaps in other cases where, as shown here, an allosteric regulatory domain can assume multiple conformations and therefore place the enzyme into more than one active conformation. This novel 2-step allosteric control of a 2-step lipid phosphatase enables voltage to shape PIP concentrations in time.

## FIGURES

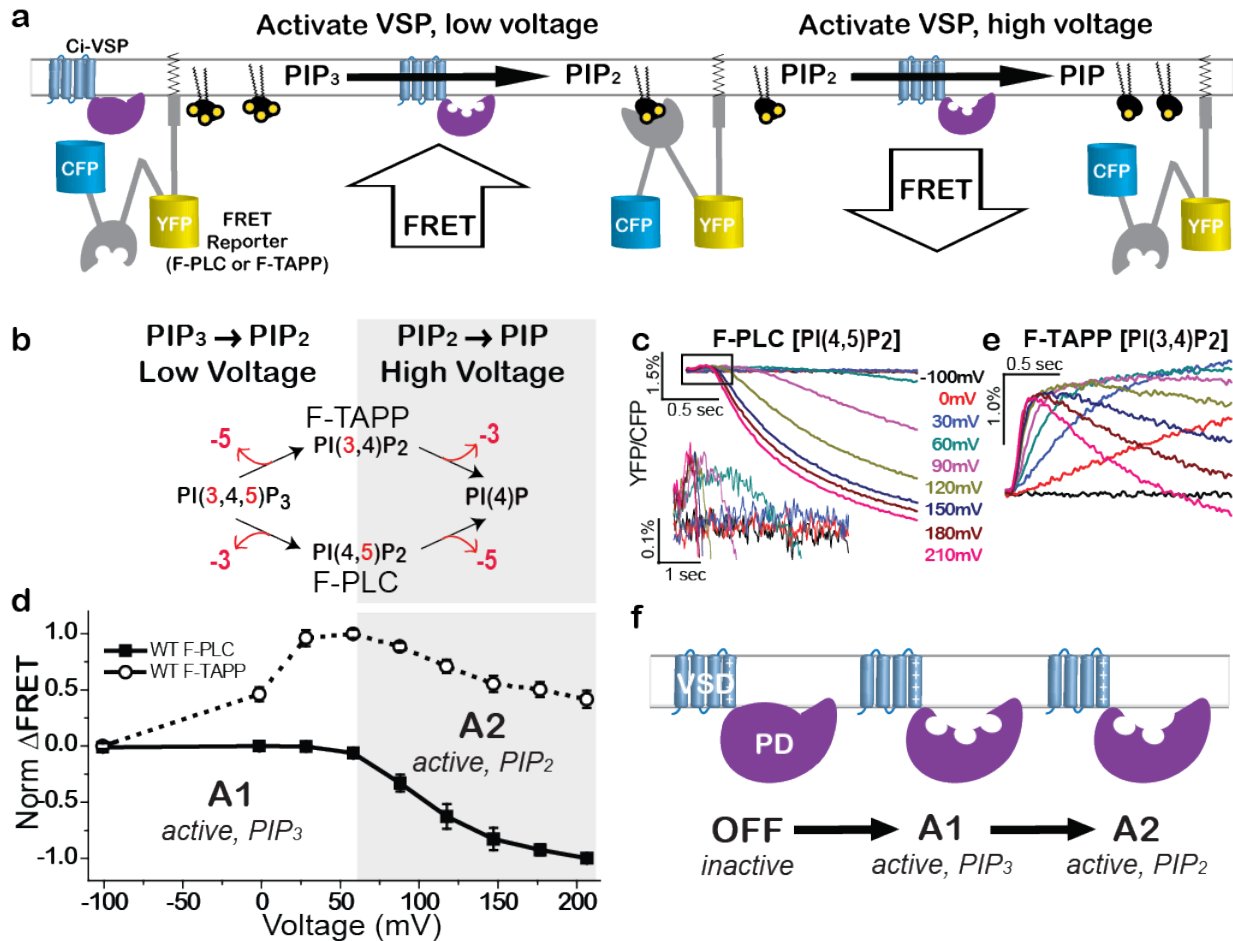


**Figure 1. Wildtype Ci-VSP appears to have two active enzymatic states.**

**a**) Schematic of FRET reporter of PIP<sub>2</sub> based on membrane-targeted pleckstrin homology (PH) domain specific for either PI(4,5)P<sub>2</sub> (PH domain from PLC; “F-PLC” reporter) or PI(3,4)P<sub>2</sub> (PH domain from TAPP; “F-TAPP” reporter). **b**) FRET protocol for monitoring specificity. **c,e**) DFRET (DYFP/DCFP) for F-PLC (left) and F-TAPP (right) in response to 2 sec depolarizing steps from V<sub>H</sub> = -100 mV. Left inset) Blowup of early phase of FRET increase for F-PLC. **d**) Normalized ΔFRET (mean ± s.e.m.; F-PLC: n=12; F-TAPP: n=17) at the end of a 2s voltage step, plotted against step voltage for F-PLC (closed squares) and F-TAPP (open circles). **f**) Schematic representing model of v-dependent control over enzyme specificity.



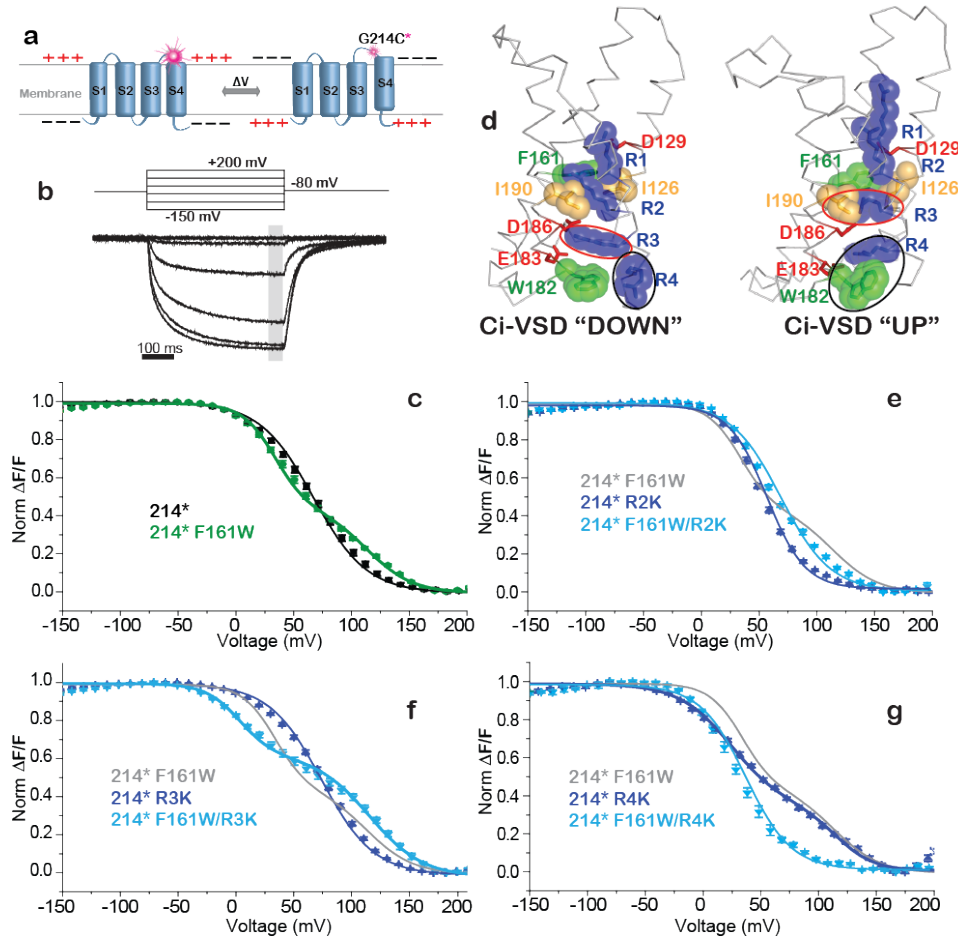


## Figure2. Stabilization of discrete conformations in the gating plug of VSD.

**a)** Cartoon depicting voltage clamp fluorometry (VCF) on the 214\* (G214C) labeling of external side of fourth helix (S4) by a dye, tetramethyl-6-maleamide (TMRM), covalently attached to introduced extracellular Cys. **b)** Positive charged residues (R1-R4) cause voltage-dependent conformational changes in S4 reported as quenching of TMRM. Mean  $\Delta F$  at end of 500ms steps (-150 to +200mV  $\Delta 10$ mV, pink) were plotted against voltage (FVs). **c)** FV curves for WT (thick black,  $67.0\text{mV} \pm 2.1$ ,  $n=11$ ), and F161W (thick red,  $33.7\text{mV} \pm 6.9$ ,  $114.13\text{mV} \pm 11.3$ ,  $n=15$ ) suggest that the plug-enlarged mutant (F161W) stabilizes an intermediate. **d)** Ci-VSD crystal structures showing R1-R4 (gating charges, blue) move past bulky (aromatic, green) and hydrophobic (orange) plug (circled, left) during transit from “DOWN” (PDB: 4G80) to “UP” (PDB: 4G7V). To stabilize an intermediate, the plug was made bulkier (F161W, S2) and gating charges were made longer and easier to trap (R1K-R4K). **e)** R2K (blue,  $56.8\text{mV} \pm 2.0$ act,  $n=6$ ) and F161W/R2K (cyan,  $68.7\text{mV} \pm 1.7$ ,  $n=6$ ) can be fit by single sigmoid, indicating R2 gating charge does not stabilize intermediate with the enlarged plug. **f)** R3K interacts with plug to stabilize an intermediate; FW/R3K has strong inflection point, and is fit by a double sigmoid (cyan,  $3.28\text{mV} \pm 6.6$ ,  $115.86\text{mV} \pm 7.15$ ,  $n=8$ ), while R3K is fit by single sigmoidal (blue,  $72.0\text{mV} \pm 2.6$ ,  $n=9$ ). **g)** F161W/R4K stabilizes an intermediate over entire range tested because the double sigmoidal FVs for the F161W and R4K (blue,  $24.22\text{mV} \pm 6.4$ ,  $115.56\text{mV} \pm 7.5$ ,  $n=8$ ) single mutants non-additively combine and lose their double sigmoidal character in FW/R4K, which was fit well by a single sigmoid (cyan,  $37.1 \pm 2.1$ ,  $n=9$ ).

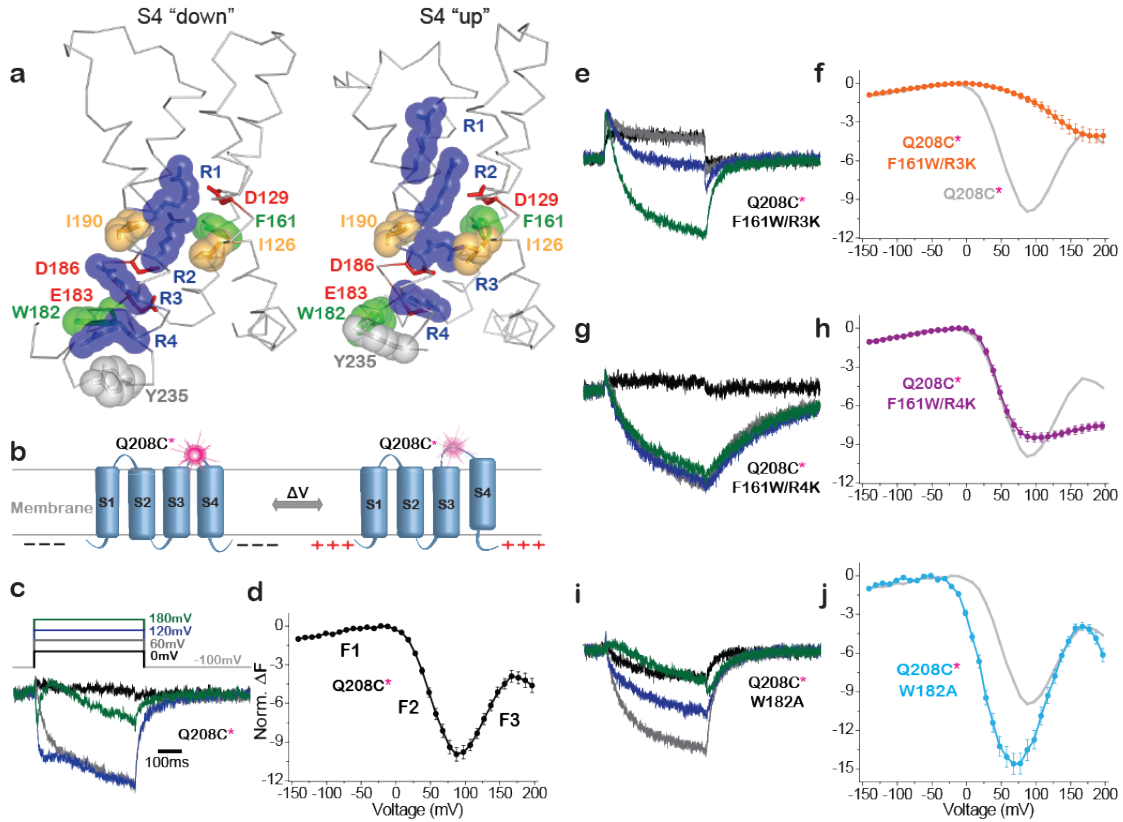


**Figure3. VSD mutants stabilize discrete VSD conformations.**

**a)** Crystal structures of VSD from WT Ci-VSP (resting at zero voltage; S4 “down”; PDB: 4G80) and R217E mutant (activated at zero voltage; S4 “up”; PDB: 4G7V) (Li et al., 2014). Deduced activation transition moves R1-R4 (blue) outward (up), with R2 crossing hydrophobic plug (I126, I190 and F161) and R4 crossing hydrophobic residue W182. **b)** Schematic of voltage clamp fluorometry with TMRM at Q208C (208\*) in S3-S4 loop. **c-j)** Fluorescence traces evoked by depolarization steps (b,d,f,g and h) and corresponding average F-Vs calculated from DF measured at end of each 500ms step (c,e,g and i). **c,d)** WT (208\*) (n=7) has three components, F1, F2 and F3. **e,f)** F161W/R3K (n=6) shifts F2 to more positive voltage and F3 out of the tested voltage range (i.e. stabilizes conformation between F1 and F2). **g,h)** F161W/R4K (n=5) has F1 and F2 but almost no F3 (i.e. stabilizes conformation between F2 and F3). **i,j)** W182A (n=7) shifts F2 and F3 to more negative voltages (i.e. easing entry into conformation between F2 and F3 and conformation after F3).

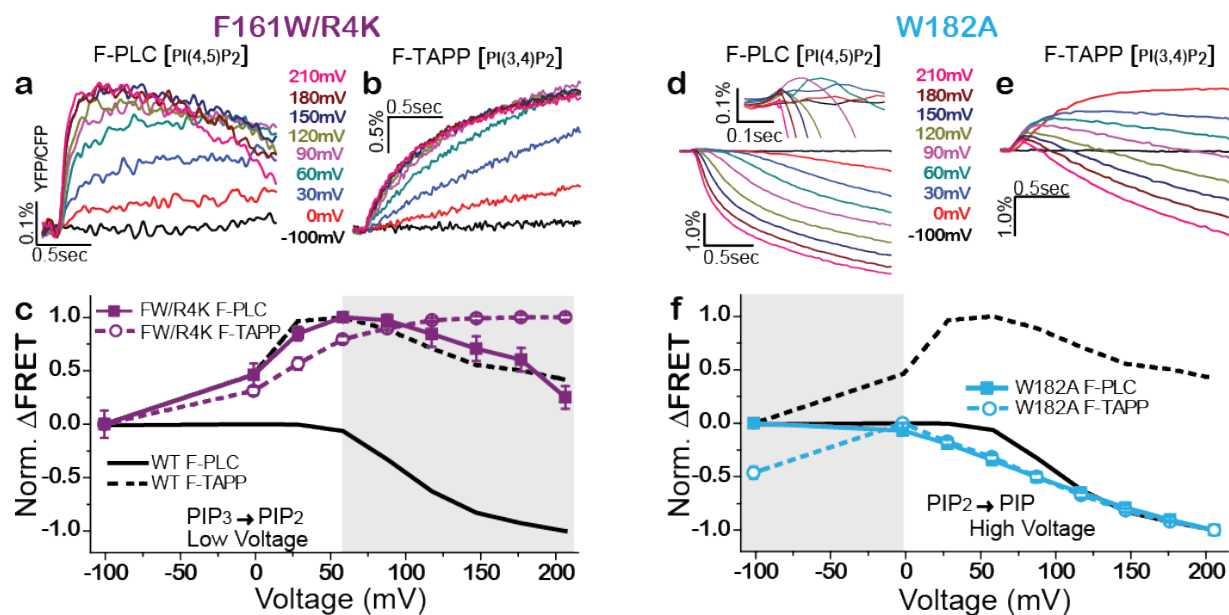


**Figure 4. VSD mutants stabilize discrete enzyme activity states.**

**a-c)** F161W/R4K favors A1 (PIP<sub>3</sub>→PIP<sub>2</sub>) enzyme activity state. F-PLC detects that F161W/R4K (a, traces; c, solid squares, n=14) augments the accumulation of PI(4,5)P<sub>2</sub> (increased FRET due to dephosphorylation of the 3-position phosphate of PI(3,4,5)P<sub>3</sub>) and suppresses the depletion of PI(4,5)P<sub>2</sub> (decreased FRET due to 5-position dephosphorylation of PI(4,5)P<sub>2</sub>) that are characteristic of WT Ci-VSP (solid grey line). F-TAPP detects that F161W/R4K (b, traces; c, open circles, n=12) augments the accumulation of PI(3,4)P<sub>2</sub> (increased FRET due to dephosphorylation of the 5-position phosphate of PI(3,4,5)P<sub>3</sub>) and suppresses the depletion of PI(3,4)P<sub>2</sub> (decreased FRET due to 5-position dephosphorylation of PI(3,4,5)P<sub>3</sub>) that are characteristic of WT Ci-VSP (dashed grey line). **d-f)** W182A shifts to more negative voltage the transition from the A1 enzyme activity state that produces accumulation of PIP<sub>2</sub> to A2 STATE that depletes of PIP<sub>2</sub> as seen in both F-PLC (d, traces; f, solid squares, n=12) and F-TAPP (e, traces; f, open circles, n=14).

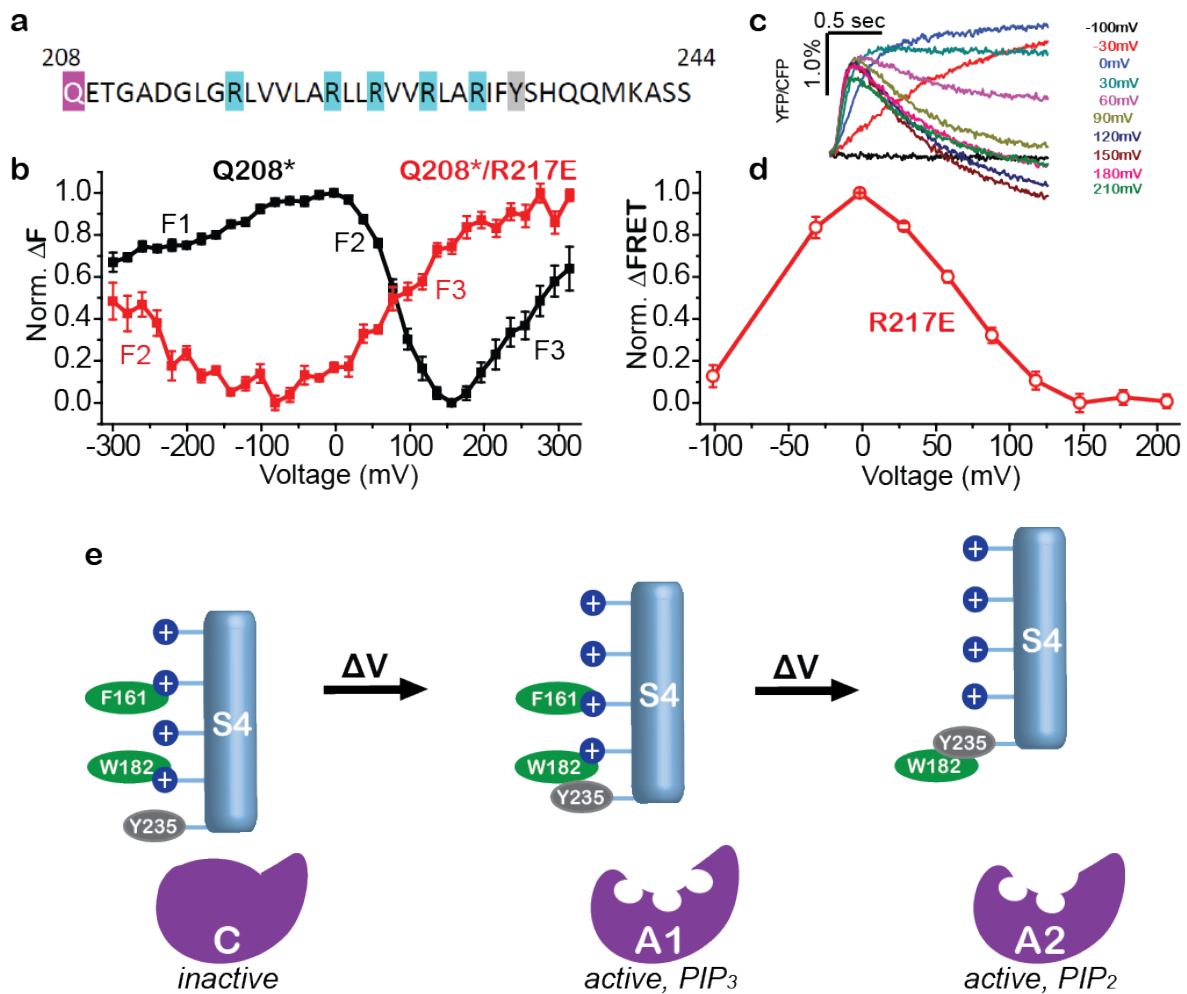
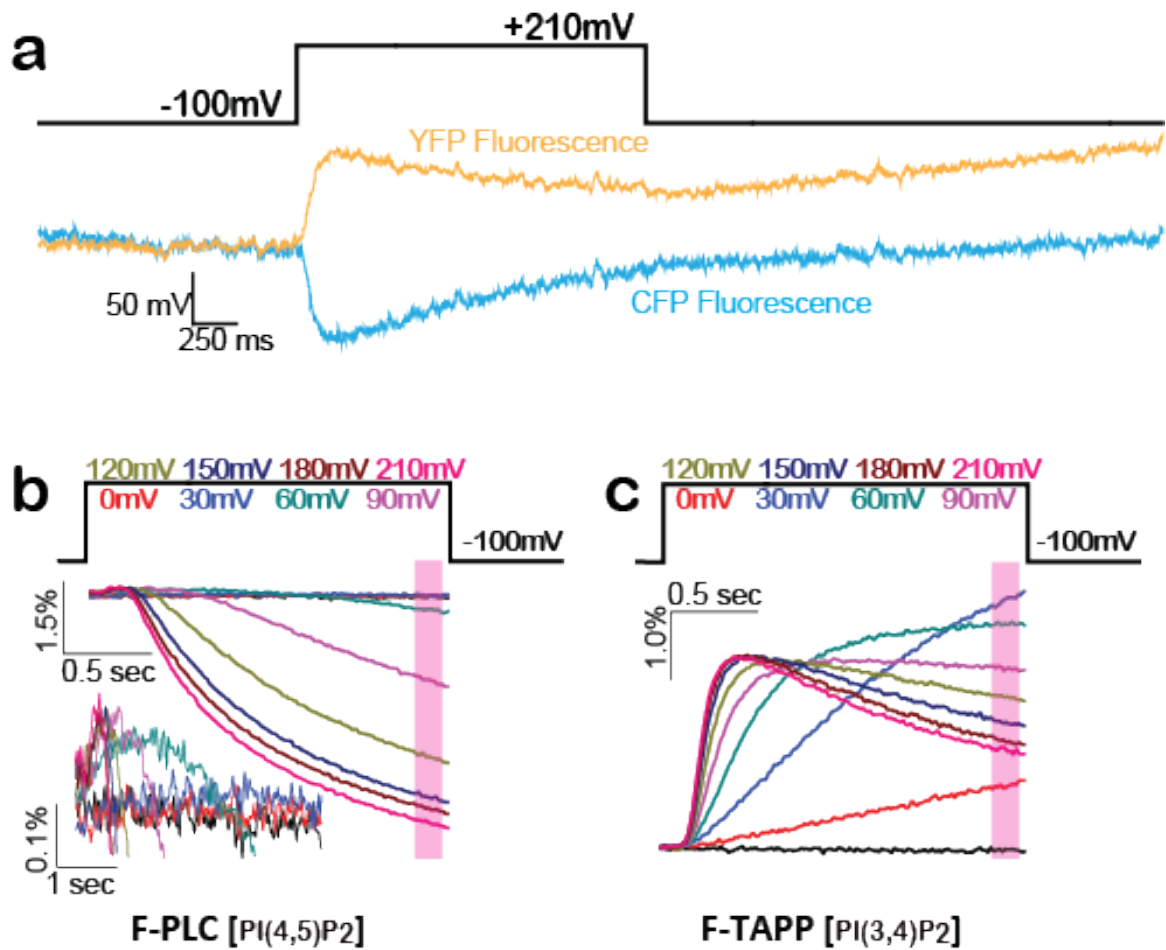


**Figure 5. Two-step VSD control over VSP phosphatase with two active states.**

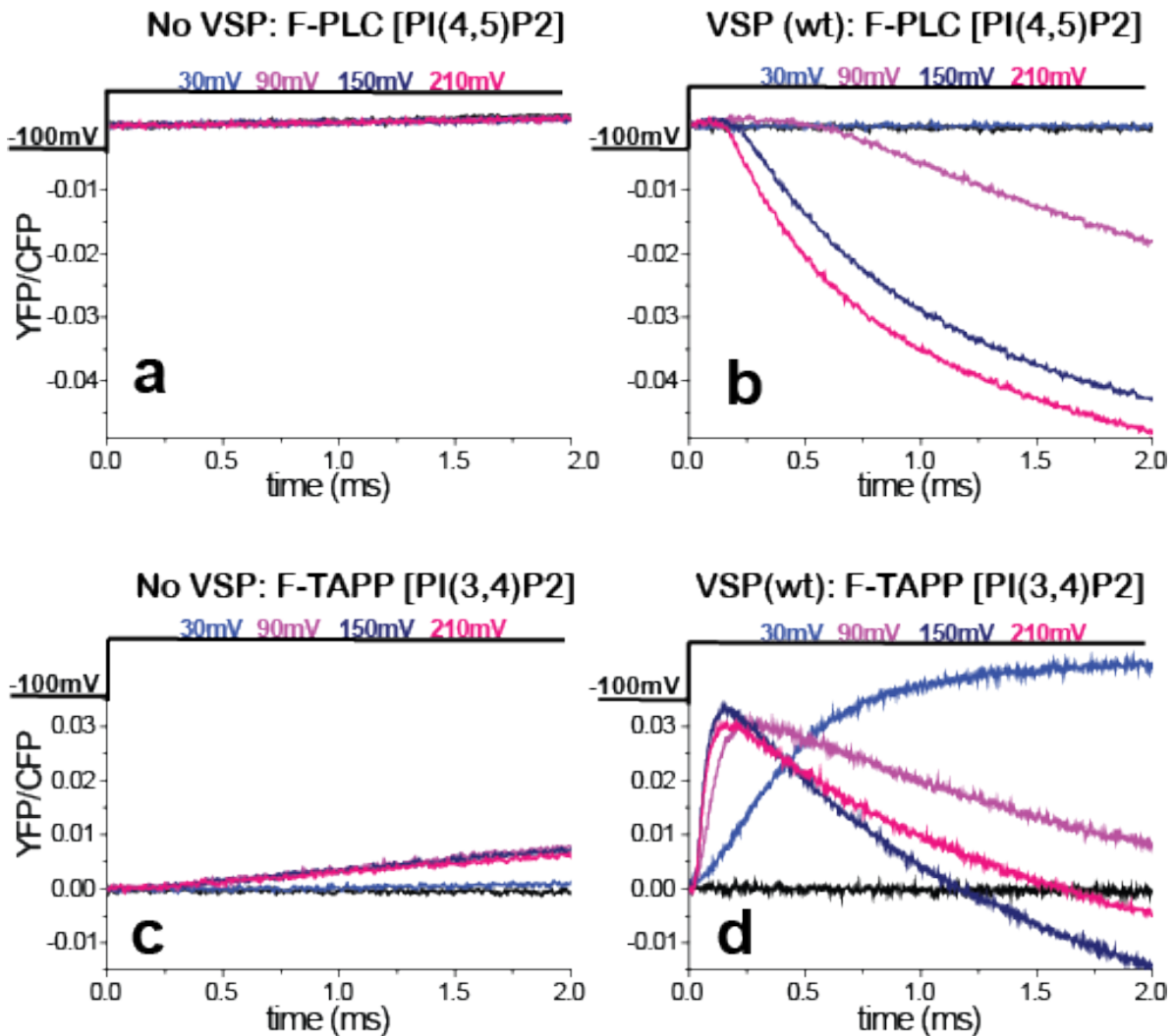
**a)** S4 sequence of with arginines (blue), including R217, whose mutation to glutamate stabilize an activated conformation of the VSD for crystallography (see Fig. 2a). **b)** F-V of Q208C-TMRM (Q208\*) shows that the R217E mutant shifts F2 and F3 in the negative direction so that zero voltage is at the F2-F3 transition. **c, d)** F-TAPP traces (c) and F-Vs (d) due to activity of WT and R217E versions of Ci-VSP show that R217E mutation shifts activity at zero voltage to maximum of  $\text{PI}(3,4,5)\text{P}_3 \rightarrow \text{PI}(3,4)\text{P}_2$  activity, suggesting that “up” structure of VSD corresponds to A1 enzyme state. **e)** Model of sequential depolarization-driven transitions in VSD that sequentially transition the phosphatase domain from inactive to the  $\text{PIP}_3$ -preferring A1 active state and then to the  $\text{PIP}_2$ -preferring A2 active state.





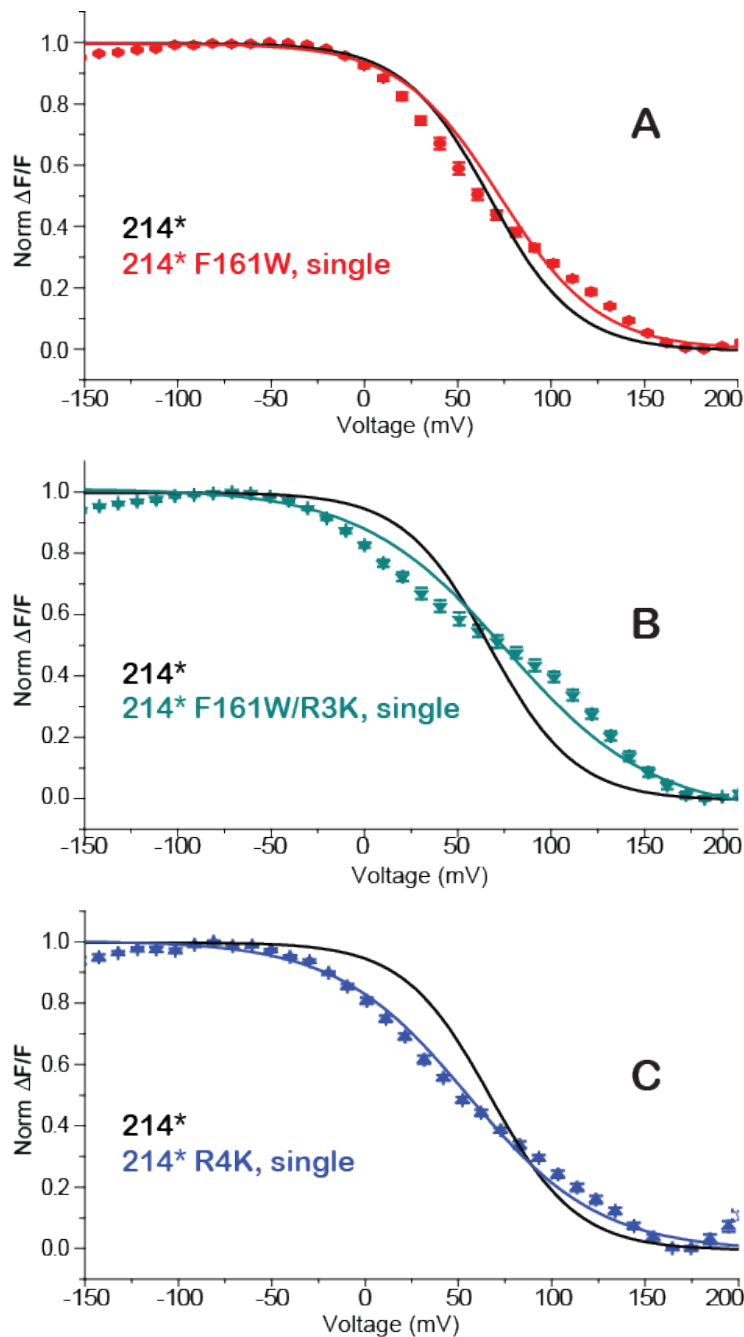
**Supplemental Figure 2. Mean change in FRET.**

**a)** YFP and CFP fluorescence was recorded for each voltage step. Ratio of YFP/CFP was calculated for each voltage and plotted versus time. **b,c)** The plots of voltage versus fluorescence (**Figure 1C/D**) were calculated from the change in YFP/CFP fluorescence at the end of the 2 second voltage step.



**Supplemental Figure 3. Endogenous Activity in Xenopus Oocytes.**

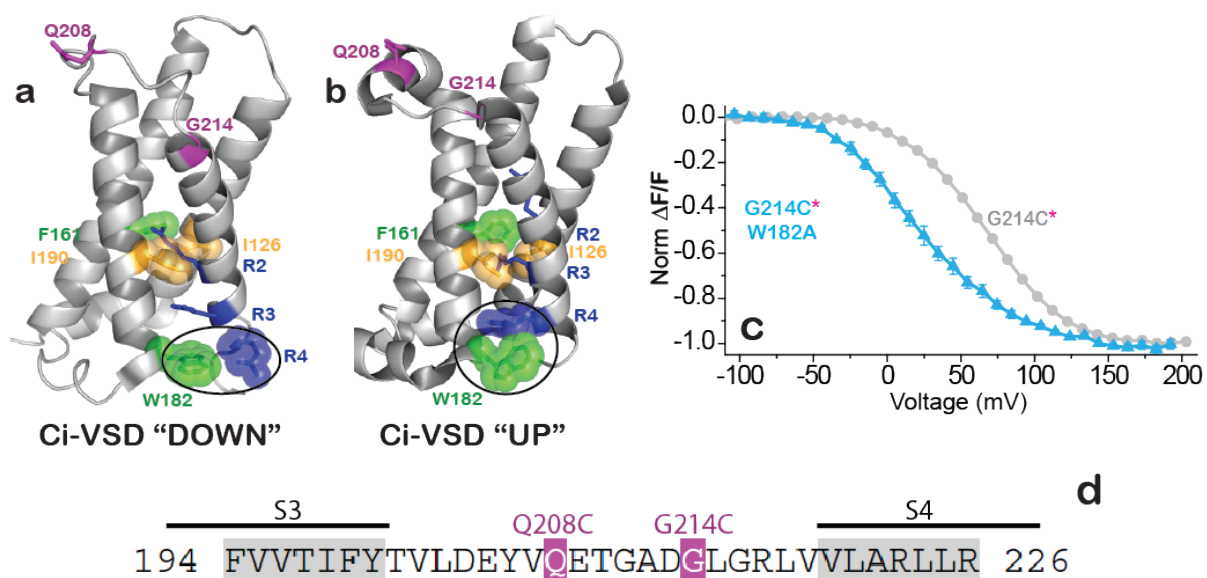
**a)** No significant voltage depletion of  $\text{PIP}_2$  is reported during the 2 second F-PLC trace. **b)** Expression of VSP (wt) with F-PLC shows that the enzyme can produce strong voltage dependent responses over the no VSP control (**Supplement 2A**). These voltages show a small increase in  $\text{PI}(4,5)\text{P}_2$ , followed by a decrease in  $\text{PI}(4,5)\text{P}_2$ . **c)** Small delayed increase in F-TAPP fluorescence indicates that an endogenous voltage dependent enzyme, possible XI-VSP, is depleting  $\text{PI}(3,4,5)\text{P}_2$  and producing  $\text{PI}(3,4)\text{P}_2$  at voltages depolarization greater than 90mV. **d)** Co-expression of Ci-VSP (214\*) with F-TAPP indicates that overexpression of VSP produces an immediate instead of delayed response (**Supplement 2C**) to depolarization, with the largest change occurring in direct response to depolarization. This evidence supports the use of short traces of 2 second or less, to monitor enzyme activity.



**Supplemental Figure4. Single sigmoidal fits for double sigmoid.**

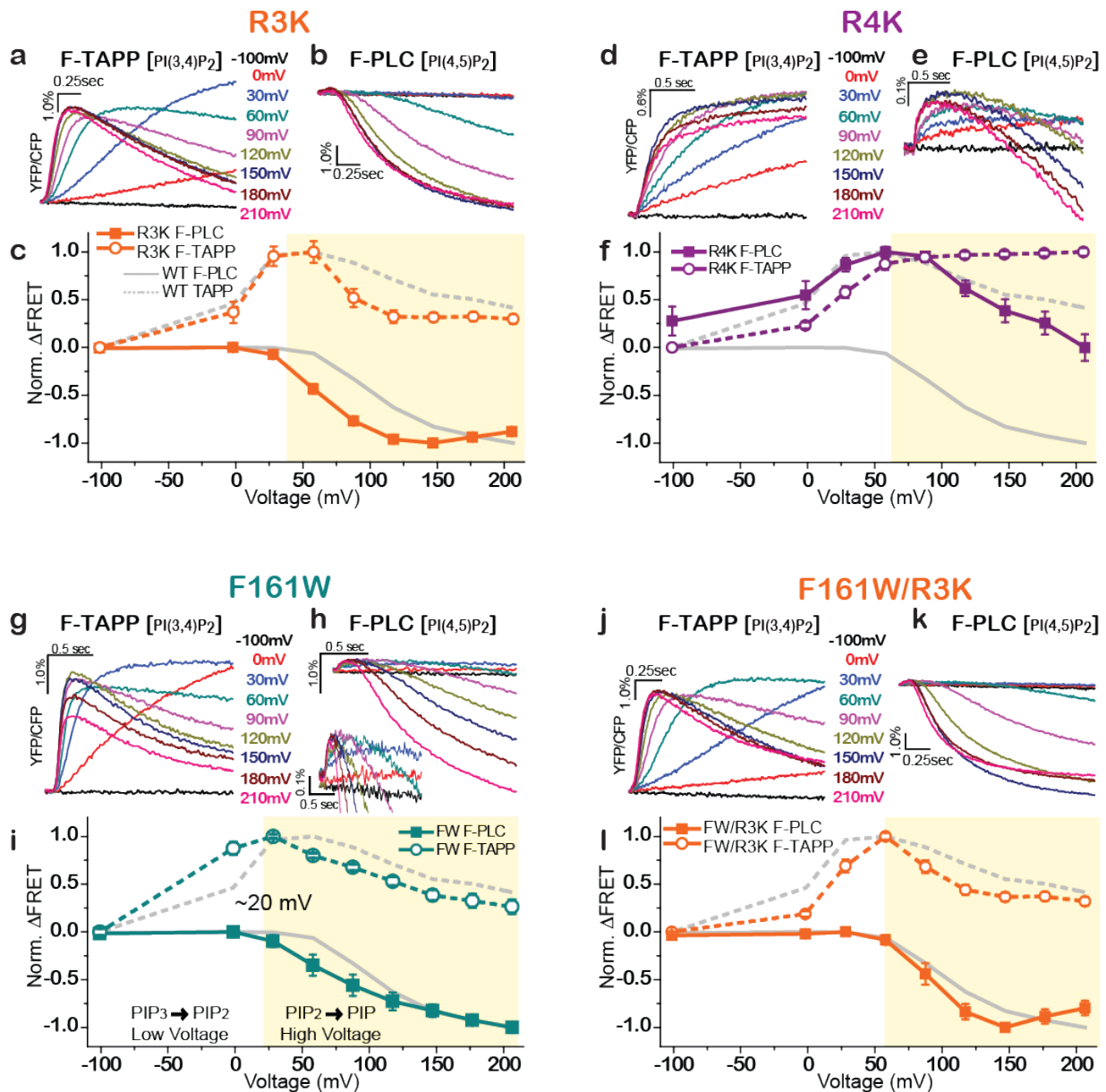
**a)** Single sigmoidal fit, red line ( $72.7 \pm 3.0$ ), is not a good fit for 214\*FW, which is clearly bi-sigmoidal. **b)** Single sigmoidal fit, green line ( $76.5 \pm 6.0$ ), is not a good fit for 214\* F161W/R3K, which is clearly bi-sigmoidal. **c)** Single sigmoidal fit, blue line ( $55.2 \pm 2.7$ ), can see the difference in fit from first and second component on either side of the single sigmoidal fit.





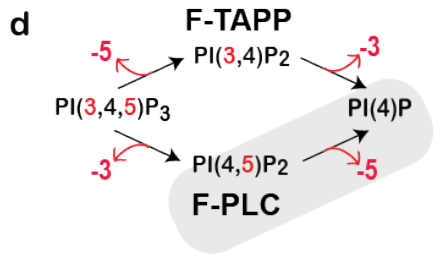
**Supplemental Figure 5. Stabilization of VSD using interactions below the VSD plug.**

**a)** In the down state of the Ci-VSD R4 is below W182, a bulky Trp on internal side of the VSD. **b)** In contrast, the up stated of the Ci-VSD shows R4 above the W182 residue. The Ci-VSD structures suggest that R4 must pass W182 to get into the up state. **c)** VCF on 214\*, which reports motions of S4, shows that W182A (214\*) is left shifted relative to wildtype (214\*); this result is consistent with the notion that R4 interacts with W182, making W182 smaller and non-aromatic (W182A) makes it easier for S4 to go into the "up" state thus shifting the FV to negative voltages. **d)** Since 214\* reports gating and motions of the fourth helix (S4), the Q208C labeling site between S3 and S4 may be an informative readout for interactions between S3 and S4.

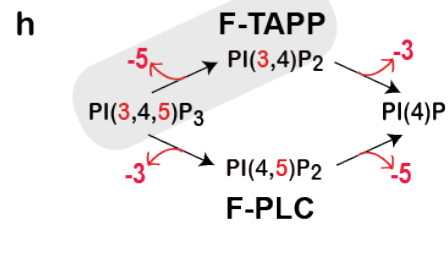


### Supplemental Figure 6. Activity data for Ci-VSP single mutants.

**a-c)** R3K is similar to WT, at voltages ~60mV PIP<sub>2</sub> is produced from PIP<sub>3</sub>, and at voltages greater than 60mV PIP<sub>2</sub> is depleted to produce PIP. (F-PLC n=9, F-TAPP n=6) **d-f)** R4K stabilizes activity on PIP<sub>3</sub> similar to FW/R4K, but at higher voltages R4K has greater PIP<sub>2</sub> depletion than FW/R4K. (F-PLC n=9, F-TAPP n=12). **g-i)** FW depletes PIP<sub>2</sub> at voltages greater than ~20mV, but has greater preference for PIP<sub>3</sub> substrate than WT. F161W (FW) alone is insufficient to more than transiently stabilize A1 state, but together with R4K strongly stabilizes the A1 state (F-TAPP n=10, F-PLC n=5). **j-k)** F161W/R3K is similar to WT, at voltages ~60mV PIP<sub>2</sub> is produced from PIP<sub>3</sub>, and at voltages greater than 60mV PIP<sub>2</sub> is depleted to produce PIP. (F-PLC n=8, F-TAPP n=14).

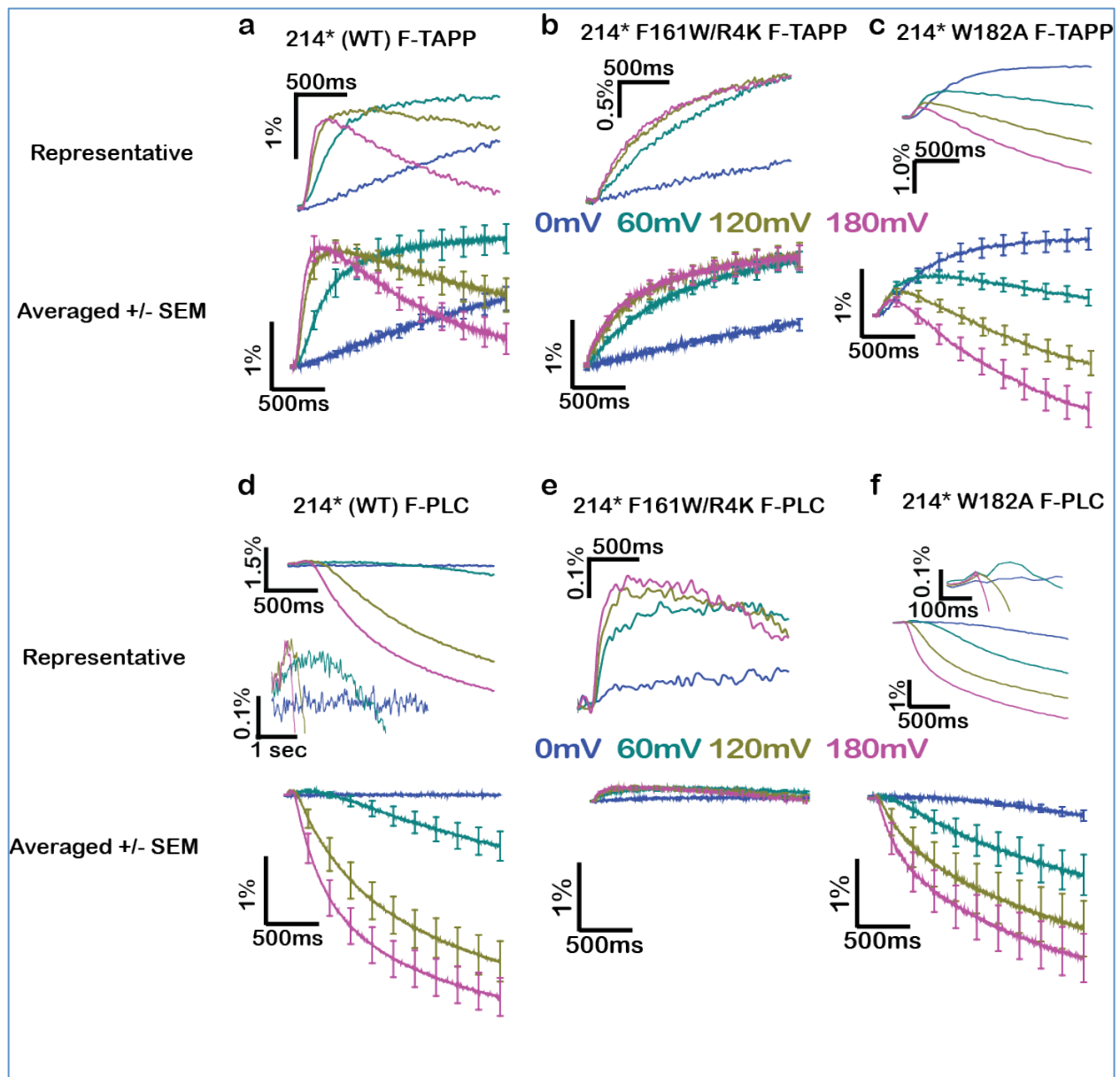


**F161W/R4K has preference for 5-activity at all voltages**



**W182A has preference for 5-activity at all voltages**

**Supplemental Figure 7. Ci-VSP has 5-position phosphatase preference at all voltages.** At high voltages, F-PLC reports 5-phosphatase activity for F161W/R4K (**Fig. 7d**), and in the W182A mutant at low voltages the F-TAPP reports 5-phosphatase activity (**Fig. 7h**). Taken together these data show that at all voltages the enzyme exhibits a preference for 5-phosphatase activity. This finding is consistent with previous reports for the enzyme (20, 21, 76, 78).



**Supplemental Figure 8. Representative traces resemble average from multiple cells.**

**a)** 214\* n=11 (fit with single); 214\* FW n=15 (fit with double, thin red line is single). **b)** 214\*R2K n=6 (fit with single), 214\*R2K FW n=6 (fit with single). **c)** 214\*R3K n=9 (fit with single), 214\*R3K FW n=8 (fit with double, thin cyan line is single). **d)** 214\*R4K n=8 (fit with double, thin blue line is single), 214\*R4K FW n=9 (fit with single).

## METHODS

### Molecular Biology.

The plasmid containing Ci-VSP in the pSD64TF vector was kindly provided by Y. Okamura (Osaka University). Ci-VSP was modified using the quick change protocol for site-specific mutagenesis which introduced the reported mutations in the voltage sensor and/or active site of the construct; mRNA produced by linearization with XbaI and SP6 transcription.

The Fllip-pm FRET reporter construct kindly provided by Michiyuki Matsuda (Kyoto University), was subcloned into the pGEMHE vector(24, 58). The GRP1-PH core domain region of the Fllip-pm construct was identified using the Conserved Domain Database (CDD) which confirmed that the construct contained two restriction enzyme sites, BspE1 and Kpn1, flanking the GRP1-PH core domain(25, 96). Similarly, we used the CDD and multiple sequence alignments of the PH-like superfamily to identify analogous core domains from TAPP1-PH kindly provided by Tamas Balla (NIH) and PLC $\delta$ 1-PH kindly provided by Tobias Meyer (Stanford University)(3, 8, 96). The identified TAPP1-PH and PLC $\delta$ 1-PH core domains were cloned out using PCR with a pair of primers that introduced the BspE1 and Kpn1 restriction sites. Finally, the GRP1-PH core domain was digested out of the Fllip-pm backbone, and a standard ligation protocol was used to replace it with either the TAPP1-PH core domain to produce F-TAPP, or the PLC $\delta$ 1-PH core domain to produce F-PLC. The resulting pGEMHE vector containing F-TAPP and F-PLC was linearized by NheI and T7 transcribed to produce mRNA for co-expression of the reporters with Ci-VSP. In response to either PI(3,4)P<sub>2</sub> or PI(4,5)P<sub>2</sub> depletion the two resulting FRET probes, F-TAPP or F-PLC respectively, produced detectable decreases in CFP fluorescence that corresponded to synchronized increases in YFP fluorescence.

### Fluorescence Measurement of Activity.

Ci-VSP mRNA and FRET reporter (F-TAPP or F-PLC) mRNA were combined at a ratio of 2:1 (0.8 $\mu$ g  $\mu$ l<sup>-1</sup> VSP: 0.4 $\mu$ g  $\mu$ l<sup>-1</sup> FRET reporter), 50nL of this mRNA mixture (~1.2  $\mu$ g  $\mu$ l<sup>-1</sup>) was injected in *Xenopus laevis* oocytes which were incubated in ND-96 (96mM NaCl, 2mM KCl, 1.8mM CaCl<sub>2</sub>, 1mM MgCl<sub>2</sub>, 50mg ml<sup>-1</sup> gentamicin, 2.5mM Na pyruvate and 5mM HEPES) media for 36-48 hours at 18° C. To limit leak during the experiment the oocytes were perfused with an NMG buffered solution (110mM N-methyl-D-glucamine (NMG) methanesulfonic acid (MS), 2mM KMS, 2mM Ca(MS)<sub>2</sub>, 10mM HEPES, pH 7.5) containing 8 $\mu$ M human recombinant Insulin (Gibco, Invitrogen) to increase PIP<sub>3</sub> concentrations in the cell.

Fluorescence detection was made through an Olympus IX-71 inverted fluorescence microscope equipped with a 20X 0.75 NA fluorescence objective (Olympus UApo/340), Uniblitz shutter (Vincent Associates), Dagan CA-1B amplifier, and a Chroma S-011335 filter cube (Olympus U-MF2) containing excitation filter (ET420nm/40nm) and dichroic (440dcrxu). The samples were illuminated by a 100W mercury arc lamp (Hamamatsu) filtered down to 25% with a neutral density filter (ND 0.6), and the emitted light was detected by a pair of PMT-100 Photomultipliers (Applied Scientific Instrumentation) attached to the left side part of the Olympus IX-71 scope through a Photoport Bean Splitter (Applied Scientific Instrumentation) equipped with a dichroic (495dcsp, Chroma Technology) and two emission filters – HQ470nm/20nm (Chroma Technology) for the CFP channel and ET535nm/30nm (Chroma Technology) for the YFP channel. A low noise acquisition system (Molecular Devices) consisting of a digitizer (Digidata-1440A) and the pClamp 10 software suite was used to control the shutter, photomultiplier tubes and the amplifier. The YFP and CFP signals from the

photomultiplier tubes were low-pass filtered at 500Hz using an eight-pole Bessel filter before being recorded by the Clampex 10 application (pClamp 10, Molecular Devices).

### **Voltage Clamp Fluorometry.**

Voltage clamp fluorometry was conducted as described in previous works(1, 3, 10, 21). *Xenopus laevis* oocytes were injected with 50nL of mRNA at 0.4-0.8 $\mu\text{g } \mu\text{l}^{-1}$  and incubated in ND-96 (96mM NaCl, 2mM KCl, 1.8mM CaCl<sub>2</sub>, 1mM MgCl<sub>2</sub>, 50mg ml<sup>-1</sup> gentamicin, 2.5mM Na pyruvate and 5mM HEPES) media for 24-48 hours at 18° C. On the day of the experiments the oocytes were incubated for 30 minutes in a high-potassium solution (92mM KCl, 0.75mM CaCl<sub>2</sub>, 1mM MgCl<sub>2</sub>, 10mM HEPES, pH 7.5) with 12 $\mu\text{M}$  tetramethylrhodamine-6-maleimide (Invitrogen). Following incubation the oocytes were subjected to multiple washing steps in ND-96 and stored in darkness at 12° C until tested.

Fluorescence detection was made through an Olympus IX-71 inverted fluorescence microscope equipped with a 20X 0.75 NA fluorescence objective (Olympus UApo/340), Uniblitz shutter (Vincent Associates), Dagan CA-1B amplifier, and Chroma U-N41002a filter cube (Chroma technology) containing an excitation filter (HQ535nm/50nm), emission filter (HQ620nm/60nm) and dichroic (Q565nm-LP). The samples were illuminated by a 100W mercury arc lamp (Hamamatsu) filtered down to 5% with a neutral density filter (ND 1.3), and the emitted light was detected by Hamamatsu HC120-05 photomultiplier tube attached to the right side part of the Olympus IX-71 scope. The Digidata-1440 low-noise acquisition system with the pClamp 10 analysis software suite (Axon Instruments) was used to control the shutter, photomultiplier tube and amplifier. The signal from the photomultiplier tube was sent through an eight-pole Bessel filter for low-pass filtering at 1kHz and collected in the Clampex 10 application within PClamp 10.

## REFERENCES

1. R. Heidelberger, M. N. Waxham, J. H. Byrne, J. L. Roberts, Eds., *From Molecules to Networks: An Introduction to Cellular and Molecular Neuroscience* (Academic Press, ed. 2, 2009).
2. C. Vogel, S. A. Teichmann, J. Pereira-Leal, The Relationship Between Domain Duplication and Recombination. *J Mol Biol* **346**, 355–365 (2005).
3. T. F. Weiss, *Cellular Biophysics, Vol. 1: Transport* (MIT Press, Cambridge, MA., 1996).
4. B. Conrad, S. E. Antonarakis, Gene Duplication: A Drive for Phenotypic Diversity and Cause of Human Disease. *Annu. Rev. Genom. Human Genet.* **8**, 17–35 (2007).
5. M. Buljan, A. Frankish, A. Bateman, Quantifying the mechanisms of domain gain in animal proteins. *Genome Biol* **11**, R74 (2010).
6. R. P. Bhattacharyya, A. Reményi, B. J. Yeh, W. A. Lim, Domains, Motifs, and Scaffolds: The Role of Modular Interactions in the Evolution and Wiring of Cell Signaling Circuits. *Annu Rev Biochem* **75**, 655–680 (2006).
7. Y. Murata, H. Iwasaki, M. Sasaki, K. Inaba, Y. Okamura, Phosphoinositide phosphatase activity coupled to an intrinsic voltage sensor. *Nature* **435**, 1239–1243 (2005).
8. P. M. Schulte, C. D. Moyes, *Principles of Animal Physiology* (Benjamin Cummings, San Francisco, ed. 1, 2005), pp. 84–89.
9. S. C. Kohout, M. H. Ulbrich, S. C. Bell, E. Y. Isacoff, Subunit organization and functional transitions in Ci-VSP. *Nat Struct Mol Biol* (2007).
10. S. C. Kohout *et al.*, Electrochemical coupling in the voltage-dependent phosphatase Ci-VSP. *Nat Methods* **6**, 369–375 (2010).
11. P. M. Castle, K. D. Zolman, S. C. Kohout, Voltage-sensing phosphatase modulation by a C2 domain. *Front Pharmacol* **6** (2015), doi:10.3389/fphar.2015.00063.
12. E. Bianconi *et al.*, An estimation of the number of cells in the human body. *Ann Hum Biol* **40**, 463–471 (2013).
13. D. Pincus, I. Letunic, P. Bork, W. A. Lim, Evolution of the phospho-tyrosine signaling machinery in premetazoan lineages. *PNAS* **105**, 9680–9684 (2008).
14. N. King *et al.*, The genome of the choanoflagellate *Monosiga brevicollis* and the origin of metazoans. *Nature* **451**, 783–788 (2008).
15. N. Yang, R. Horn, Evidence for voltage-dependent S4 movement in sodium channels. *Neuron* **15**, 213–218 (1995).

16. W. A. Lim, T. Pawson, Phosphotyrosine Signaling: Evolving a New Cellular Communication System. *Cell* **142**, 661–667 (2010).
17. W. Lim, B. Mayer, T. Pawson, *Cell Signaling: principles and mechanisms* (Taylor & Francis, 2014).
18. K. A. Sutton, M. K. Jungnickel, L. Jovine, H. M. Florman, Evolution of the Voltage Sensor Domain of the Voltage-Sensitive Phosphoinositide Phosphatase VSP/TPTE Suggests a Role as a Proton Channel in Eutherian Mammals. *Molecular Biology and Evolution* **29**, 2147–2155 (2012).
19. C. R. Halaszovich, D. N. Schreiber, D. Oliver, Ci-VSP Is a Depolarization-activated Phosphatidylinositol-4,5-bisphosphate and Phosphatidylinositol-3,4,5-trisphosphate 5'-Phosphatase. *J Biol Chem* **284**, 2106–2113 (2009).
20. T. Kurokawa *et al.*, 3' Phosphatase activity toward phosphatidylinositol 3,4-bisphosphate [PI(3,4)P<sub>2</sub>] by voltage-sensing phosphatase (VSP). **109**, 10089–10094 (2012).
21. L. Liu *et al.*, A glutamate switch controls voltage-sensitive phosphatase function. *Nat Struct Mol Biol* **19**, 633–641 (2012).
22. K. Hobiger, T. Friedrich, Voltage sensitive phosphatases: emerging kinship to protein tyrosine phosphatases from structure–function research. *Front Pharmacol* **6**, 20 (2015).
23. G. Di Paolo, P. De Camilli, Phosphoinositides in cell regulation and membrane dynamics. *Nature* **443**, 651–657 (2006).
24. R. Pulido, R. H. van Huijsduijnen, Protein tyrosine phosphatases: dual-specificity phosphatases in health and disease. *FEBS Journal* **275**, 848–866 (2008).
25. E. Marban, G. F. Tomaselli, Ion channels as enzymes: analogy or homology? *Trends in Neurosciences* **20**, 144–147 (1997).
26. B. Hille, E. J. Dickson, M. Kruse, O. Vivas, B.-C. Suh, *Biochimica et Biophysica Acta. (BBA) - Molecular and Cell Biology of Lipids* **1851**, 844–856 (2015).
27. A. L. Hodgkin, A. F. Huxley, A quantitative description of membrane current and its application to conduction and excitation in nerve. *J Physiol* **117**, 500–544 (1952).
28. C. M. Armstrong, F. Bezanilla, Currents related to movement of the gating particles of the sodium channels. *Nature* **242**, 459–461 (1973).
29. R. B. Campbell, F. Liu, A. H. Ross, Allosteric Activation of PTEN Phosphatase by Phosphatidylinositol 4,5-Bisphosphate. *J Biol Chem* **278**, 33617–33620 (2003).
30. L. Mannuzzu, M. Moronne, E. Y. Isacoff, Direct physical measure of conformational rearrangement underlying potassium channel gating. *Science* (1996).



31. H. Iwasaki *et al.*, A voltage-sensing phosphatase, Ci-VSP, which shares sequence identity with PTEN, dephosphorylates phosphatidylinositol 4,5-bisphosphate. *PNAS* **105**, 7970–7975 (2008).
32. J. Lacroix *et al.*, Controlling the Activity of a Phosphatase and Tensin Homolog (PTEN) by Membrane Potential. *J Biol Chem* **286**, 17945–17953 (2011).
33. F. Tombola, M. Pathak, E. Y. Isacoff, How does voltage open an ion channel? *Annu Rev Cell Dev Biol* (2006).
34. F. Tombola, M. Pathak, P. Gorostiza, E. Y. Isacoff, The twisted ion-permeation pathway of a resting voltage-sensing domain. *Nature* (2006).
35. E. Y. Isacoff, L. Y. Jan, D. L. Minor Jr, Perspective. *Neuron* **80**, 658–674 (2013).
36. Y. Okamura, Biodiversity of voltage sensor domain proteins. *Pflügers Archiv European Journal of Physiology* **454**, 361–371 (2007).
37. E. Palovcak, L. Delemotte, M. L. Klein, V. Carnevale, Evolutionary imprint of activation: The design principles of VSDs. *J Gen Physiol* **143**, 145–156 (2014).
38. C. Gandhi, E. Y. Isacoff, Molecular models of voltage sensing. *J Gen Physiol* (2002).
39. H. Lecar, H. P. Larsson, M. Grabe, Electrostatic Model of S4 Motion in Voltage-Gated Ion Channels. *Biophys J* **85**, 2854–2864 (2003).
40. R. Horn, How S4 Segments Move Charge. Let Me Count the Ways. *J Gen Physiol* **123**, 1–4 (2003).
41. M. Pathak, L. Kurtz, F. Tombola, E. Y. Isacoff, The cooperative voltage sensor motion that gates a potassium channel. *J Gen Physiol* (2005).
42. D. D. Brown, A Tribute to the *Xenopus laevis* Oocyte and Egg. *J Biol Chem* **279**, 45291–45299 (2004).
43. E. Loots, E. Y. Isacoff, Protein rearrangements underlying slow inactivation of the Shaker K<sup>+</sup> channel. *J Gen Physiol* **112**, 377–389 (1998).
44. L. Mannuzzu, E. Y. Isacoff, Independence and cooperativity in rearrangements of a potassium channel voltage sensor revealed by single subunit fluorescence. *J Gen Physiol* (2000).
45. M. M. Pathak *et al.*, Closing In on the Resting State of the Shaker K<sup>+</sup> Channel. *Neuron* **56**, 124–140 (2007).
46. C. A. Villalba-Galea *et al.*, Charge Movement of a Voltage-Sensitive Fluorescent Protein. *Biophys J* **96**, L19–L21 (2009).
47. C. A. Villalba-Galea, W. Sandtner, D. M. Starace, F. Bezanilla, Inaugural Article: S4-

- based voltage sensors have three major conformations. *PNAS* **105**, 17600–17607 (2008).
48. S. Aggarwal, R. MacKinnon, Contribution of the S4 segment to gating charge in the Shaker K<sup>+</sup> channel. *Neuron* **16**, 1169–1177 (1996).
  49. S. Seoh, D. Sigg, D. Papazian, Voltage-sensing residues in the S2 and S4 segments of the Shaker K<sup>+</sup> channel. *Neuron* (1996).
  50. O. S. Baker, H. P. Larsson, L. M. Mannuzzu, E. Y. Isacoff, Three transmembrane conformations and sequence-dependent displacement of the S4 domain in shaker K<sup>+</sup> channel gating. *Neuron* **20**, 1283–1294 (1998).
  51. C. S. Gandhi *et al.*, Reconstructing voltage sensor-pore interaction from a fluorescence scan of a voltage-gated K<sup>+</sup> channel. *Neuron* **27**, 585–595 (2000).
  52. C. A. Villalba-Galea, F. Miceli, M. Tagliatalata, F. Bezanilla, Coupling between the voltage-sensing and phosphatase domains of Ci-VSP. *J Gen Physiol* **134**, 5–14 (2009).
  53. C. S. Schwaiger, P. Bjelkmar, B. Hess, E. Lindahl, 310-Helix Conformation Facilitates the Transition of a Voltage Sensor S4 Segment toward the Down State. *Biophys J* **100**, 1446–1454 (2011).
  54. T. Balla, Phosphoinositides: Tiny Lipids With Giant Impact on Cell Regulation. *Physiol Rev* **93**, 1019–1137 (2013).
  55. F. Hsu, Y. Mao, *Biochimica et Biophysica Acta. (BBA) - Molecular and Cell Biology of Lipids* **1851**, 698–710 (2015).
  56. C. L. Huang, Complex roles of PIP<sub>2</sub> in the regulation of ion channels and transporters. *Am J Physiol Renal Physiol* **293**, F1761–F1765 (2007).
  57. B.-C. Suh, B. Hille, PIP<sub>2</sub> is a necessary cofactor for ion channel function: how and why? *Annu Rev Biophys* **37**, 175–195 (2008).
  58. M. Sato, Y. Ueda, T. Takagi, Y. Umezawa, Production of PtdInsP<sub>3</sub> at endomembranes is triggered by receptor endocytosis. *Nat Cell Biol* **5**, 1016–1022 (2003).
  59. T. Maehama, G. S. Taylor, J. E. Dixon, PTEN and myotubularin: novel phosphoinositide phosphatases. *Annu Rev Biochem* **70**, 247–279 (2001).
  60. Z.-Y. Zhang, PROTEIN TYROSINE PHOSPHATASES: Structure and Function, Substrate Specificity, and Inhibitor Development. *Annu. Rev. Pharmacol. Toxicol.* **42**, 209–234 (2002).
  61. T. A. S. Brandao, A. C. Hengge, S. J. Johnson, Insights into the Reaction of Protein-tyrosine Phosphatase 1B: CRYSTAL STRUCTURES FOR TRANSITION STATE ANALOGS OF BOTH CATALYTIC STEPS. *J Biol Chem* **285**, 15874–15883 (2010).

62. J. den Hertog, Regulation of protein phosphatases in disease and behaviour. *EMBO Rep* **4**, 1027–1032 (2003).
63. Y. Liu, V. A. Bankaitis, Phosphoinositide phosphatases in cell biology and disease. *Progress in Lipid Research* **49**, 201–217 (2010).
64. R. Pulido, A. W. Stoker, W. J. A. J. Hendriks, PTPs emerge as PIPs: protein tyrosine phosphatases with lipid-phosphatase activities in human disease. *Human Molecular Genetics* **22**, R66–R76 (2013).
65. J. Lacroix *et al.*, Controlling the activity of PTEN by membrane potential. *J Biol Chem* (2011).
66. J. Patti, E. Y. Isacoff, Measuring membrane voltage with fluorescent proteins. *Cold Spring Harb Protoc* **2013**, 606–613 (2013).
67. H. H. Piao, D. Rajakumar, B. E. Kang, E. H. Kim, B. J. Baker, Combinatorial Mutagenesis of the Voltage-Sensing Domain Enables the Optical Resolution of Action Potentials Firing at 60 Hz by a Genetically Encoded Fluorescent Sensor of Membrane Potential. *J Neurosci* **35**, 372–385 (2015).
68. F. St-Pierre *et al.*, teChnICal repOrtS. *Nature Publishing Group* **17**, 884–889 (2014).
69. H. N. Motlagh, J. O. Wrabl, J. Li, V. J. Hilser, The ensemble nature of allostery. *Nature* **508**, 331–339 (2014).
70. J. Monod, F. Jacob, Teleonomic mechanisms in cellular metabolism, growth, and differentiation. *Cold Spring Harb Symp Quant Biol* **26**, 389–401 (1961).
71. J. P. Changeux, The feedback control mechanisms of biosynthetic L-threonine deaminase by L-isoleucine. *Cold Spring Harb Symp Quant Biol* **26**, 313–318 (1961).
72. J. Monod, J. WYMAN, J. P. Changeux, ON THE NATURE OF ALLOSTERIC TRANSITIONS: A PLAUSIBLE MODEL. *J Mol Biol* **12**, 88–118 (1965).
73. V. J. Hilser, An Ensemble View of Allostery. *Science* **327**, 653–654 (2010).
74. C. A. Worby, Phosphoinositide phosphatases: emerging roles as voltage sensors? *Mol Interv* **5**, 274–277 (2005).
75. Y. Murata, Y. Okamura, Depolarization activates the phosphoinositide phosphatase Ci-VSP, as detected in *Xenopus* oocytes coexpressing sensors of PIP<sub>2</sub>. *J Physiol* **583**, 875–889 (2007).
76. C. R. Halaszovich, D. N. Schreiber, D. Oliver, Ci-VSP Is a Depolarization-activated Phosphatidylinositol-4,5-bisphosphate and Phosphatidylinositol-3,4,5-trisphosphate 5'-Phosphatase. *J Biol Chem* **284**, 2106–2113 (2008).

77. M. Matsuda *et al.*, Crystal structure of the cytoplasmic phosphatase and tensin homolog (pten)-like region of ciona intestinalis voltage-sensing phosphatase provides insight into substrate specificity and redox regulation of the phosphoinositide phosphatase activity. *J Biol Chem* **286**, 23368–23377 (2011).
78. S. Sakata, Y. Okamura, Phosphatase activity of the voltage-sensing phosphatase, VSP, shows graded dependence on the extent of activation of the voltage sensor. *J Physiol* **592**, 899–914 (2014).
79. A. Cha, F. Bezanilla, Characterizing Voltage-Dependent Conformational Changes in the ShakerK<sup>+</sup> Channel with Fluorescence. *Neuron* **19**, 1127–1140 (1997).
80. B. Chanda, O. Asamoah, R. Blunck, Gating charge displacement in voltage-gated ion channels involves limited transmembrane movement. *Nature* (2005).
81. H. P. Koch *et al.*, Multimeric nature of voltage-gated proton channels. *PNAS* **105**, 9111–9116 (2008).
82. A. Chamberlin *et al.*, Hydrophobic plug functions as a gate in voltage-gated proton channels. *PNAS* **111**, E273–E282 (2014).
83. J. J. Lacroix, F. Bezanilla, Control of a final gating charge transition by a hydrophobic residue in the S2 segment of a K<sup>+</sup> channel voltage sensor. *PNAS* **108**, 6444–6449 (2011).
84. D. M. Papazian *et al.*, Electrostatic interactions of S4 voltage sensor in Shaker K<sup>+</sup> channel. *Neuron* **14**, 1293–1301 (1995).
85. D. M. Papazian, L. C. Timpe, Y. N. Jan, L. Y. Jan, Alteration of voltage-dependence of Shaker potassium channel by mutations in the S4 sequence. *Nature* **349**, 305–310 (1991).
86. W. A. Catterall, Molecular properties of voltage-sensitive sodium channels. *Annu Rev Biochem* **55**, 953–985 (1986).
87. H. R. Guy, P. Seetharamulu, Molecular model of the action potential sodium channel. *PNAS* **83**, 508–512 (1986).
88. L. Hong, I. H. Kim, F. Tombola, Molecular determinants of Hv1 proton channel inhibition by guanidine derivatives. *PNAS* **111**, 9971–9976 (2014).
89. J. J. Lacroix, H. C. Hyde, F. V. Campos, F. Bezanilla, Moving gating charges through the gating pore in a Kv channel voltage sensor. *PNAS* **111**, E1950–E1959 (2014).
90. S. A. Pless *et al.*, Asymmetric functional contributions of acidic and aromatic side chains in sodium channel voltage-sensor domains. *J Gen Physiol* **143**, 645–656 (2014).
91. Y. M. Cheng *et al.*, Functional interactions of voltage sensor charges with an S2 hydrophobic plug in hERG channels. *J Gen Physiol* **142**, 289–303 (2013).

92. J. J. Lacroix *et al.*, Intermediate state trapping of a voltage sensor. *J Gen Physiol* **140**, 635–652 (2012).
93. S. A. Pless, J. D. Galpin, A. P. Niciforovic, C. A. Ahern, Contributions of counter-charge in a potassium channel voltage-sensor domain. *Nat Chem Biol* **7**, 617–623 (2011).
94. X. Tao, A. Lee, W. Limapichat, D. A. Dougherty, R. MacKinnon, A Gating Charge Transfer Center in Voltage Sensors. *Science* **328**, 67–73 (2010).
95. Q. Li *et al.*, Structural mechanism of voltage-dependent gating in an isolated voltage-sensing domain. *Nat Struct Mol Biol* **21**, 244–252 (2014).
96. A. Marchler-Bauer *et al.*, CDD: a Conserved Domain Database for the functional annotation of proteins. *Nucleic Acids Res* **39**, D225–9 (2011).